# DEVELOPMENT OF A NOVEL LASER MATERIAL FOR MINIATURIZED LASER SYSTEMS

FINAL TECHNICAL REPORT

8 November 1980 to 31 December 1981

Sponsored by

DEFENSE ADVANCED RESEARCH PROJECTS AGENCY

DARPA Order No. 4040

Contract No. MDA903-81-C-0034

Principal Investigator: Dr. Walter Zwicker (914) 762-0300

Monitored by: James Gibson

Contract Period: 8 Nov. 1980 - 31 Dec. 1981









Prepared by

PHILIPS LABORATORIES
A Division of North American Philips Corporation
Briarcliff Manor, New York 10510

May 19

UNCLASSIFIED

SECURITY CLASSIFICATION OF THIS PAGE (When Data Entered)

| REPORT DOCUMENTATION PAGE | READ INSTRUCTIONS BEFORE COMPLETING FORM |
|---|---|
| 1. REPORT NUMBER | 2. GOVT ACCESSION NO. AD-A119 457 | 3. RECIPIENT'S CATALOG NUMBER |
| 4. TITLE (and Subtitle) DEVELOPMENT OF A NOVEL LASER MATERIAL FOR MINIATURIZED LASER SYSTEMS | 5. TYPE OF REPORT & PERIOD COVERED Final Technical Report 8 Nov. 1980 - 31 Dec. 1981 |
| | 6. PERFORMING ORG. REPORT NUMBER |
| 7. AUTHOR(s) Walter Zwicker Sel Colak | 8. CONTRACT OR GRANT NUMBER(s) MDA903-81-C-0034 |
| 9. PERFORMING ORGANIZATION NAME AND ADDRESS PHILIPS LABORATORIES A Division of North American Philips Corp. Briarcliff Manor, New York 10510 | 10. PROGRAM ELEMENT, PROJECT, TASK AREA & WORK UNIT NUMBERS |
| 11. CONTROLLING OFFICE NAME AND ADDRESS Defense Advanced Research Projects Agency 1400 Wilson Boulevard Arlington, Virginia 22209 | 12. REPORT DATE May 1982 |
| | 13. NUMBER OF PAGES 51 |
| 14. MONITORING AGENCY NAME & ADDRESS(if different from Controlling Office) | 15. SECURITY CLASS. (of this report) UNCLASSIFIED |
| | 15a. DECLASSIFICATION/DOWNGRADING SCHEDULE |

16. DISTRIBUTION STATEMENT (of this Report)

APPROVED FOR PUBLIC RELEASE
DISTRIBUTION UNLIMITED

17. DISTRIBUTION STATEMENT (of the abstract entered in Block 20, if different from Report)

all subscripts, please !!!

18. SUPPLEMENTARY NOTES

19. KEY WORDS (Continue on reverse side if necessary and identify by block number)

Laser materials
Miniature lasers
Crystal growth
Laser rods
Stoichiometric neodymium compounds
Laser cavity
Stoichiometric erbium compounds

please

20. ABSTRACT (Continue on reverse side if necessary and identify by block number)

Single crystals of $NdP_5O_{14}$, $NdLiP_4O_{12}$, and $NdAl_3(BO_3)_4$ were grown from various type of fluxes. Miniature laser rods up to 2 x 2 x 20 mm in size were fabricated from crystals of $NdP_5O_{14}$. The spectroscopic properties of these compounds are compared, and data are given of the lasing experiments with $NdP_5O_{14}$ on laser pulse energies, pulse shapes, and beam divergences at different repetition rates with and without Q-switching. Single-pulse output energies up to 240 mJ in the free-oscillation mode

DD FORM 1 JAN 73 1473 EDITION OF 1 NOV 65 IS OBSOLETE

UNCLASSIFIED

SECURITY CLASSIFICATION OF THIS PAGE (When Data Entered)

20. ABSTRACT (Cont'd.)

and up to 30 mJ in the Q-switched mode were obtained. Repetitive pulsed operation was possible at rates of 5-10 pps with forced gas cooling. Single crystals of $(RE)P_5O_{14}$, $(RE)LiP_4O_{12}$, and $(RE)Al_3(BO_3)_4$ with $Er^{3+}$, as well as with Gd and Yb, were grown and studied spectroscopically. The data shows that these materials have $Er^{3+}$ luminescence properties similar to those of $Er^{3+}$ in other hosts which have shown lasing. $4I_{13/2}$ levels show strong luminescence at 1.55 $\mu$m with lifetimes in the order of milliseconds, and $4S_{3/2}$ levels show quenching at 1.7 $\mu$m which results in fluorescence lifetimes in the order of microseconds. The approximate emission cross sections of these transitions are given.

## SUMMARY

The original goal of this contract was the development of a novel laser material for a miniaturized laser system emitting at 1.05 to 1.06 $\mu$m. Since stoichiometric neodymium (Nd) compounds are ideally suited for this application, $NdP_5O_{14}$, $NdLiP_4O_{12}$, and $NdAl_3(BO_3)_4$ were selected as the most promising candidates from all better-known, novel stoichiometric neodymium compounds. Crystals of these three compounds were grown successfully from fluxed melts. The $NdP_5O_{14}$ crystals were by far the largest (up to 35 mm in cross section) and were of superior optical quality. Our work was, therefore, concentrated on this compound. Laser rods 2 x 2 x 20 mm in size were fabricated from these crystals. In July 1981, the goals and duration of the program were modified to include the crystal growth and optical evaluation of stoichiometric erbium compounds for miniature lasers emitting in the eye-safe region of the spectrum. Crystals of $ErP_5O_{14}$, $ErLiP_4O_{12}$, and $ErAl_3(BO_3)_4$ with partial replacement of Er by Gd or Yb were grown from fluxed melts.

The optical studies on crystals containing $Nd^{3+}$ or $Er^{3+}$ were directed towards understanding the spectroscopic properties of these materials for lasing applications. The spectroscopic properties of $NdP_5O_{14}$, $NdLiP_4O_{12}$, and $NdAl_3(BO_3)_4$ were compared, and data are given of the lasing experiments with various $NdP_5O_{14}$ laser rods. These lasing experiments have shown that the experimental $NdP_5O_{14}$ laser rods with 2 x 2 x 20 mm dimensions are capable of output energies up to 240 mJ in the free-oscillation mode with flashlamp pumping. In the Q-switched mode with a passive Q-switch, similar experiments resulted in output energies up to 30 mJ, and pulse lengths of about 15 ns at FWHM were achieved at lower output energies. In cavities with nearly confocal configuration, similar-size $NdP_5O_{14}$ crystals lased at pulse repetition rates up to 5 pps for a total of about 50 pulses. Up to 1 minute operation at 10 pps was possible only by forced argon-gas cooling of the crystal, but in these experiments the average pulse energy was low. The output-beam divergence properties of the $NdP_5O_{14}$ laser were measured in a cavity with nearly flat mirrors, and the far-field beam angle was about 2 mrad. In all laser experiments, no failure due to mechanical and/or thermal loading was observed.

The stoichiometric crystals containing $Er^{3+}$ were evaluated only spectroscopically for possible eye-safe laser applications. The fluorescence lifetimes and emission cross section of $Er^{3+}$ in these crystals are similar to that observed for $Er^{3+}$ in other hosts which showed lasing both at the $^4S_{3/2}$ --> $^4I_{9/2}$ and $^4I_{13/2}$ --> $^4I_{15/2}$ transitions. These transitions in $ErP_5O_{14}$, $ErLiP_4O_{12}$, and $ErAl_3(BO_3)_4$ are nearly in resonance, causing the cross relaxation of $^4S_{3/2}$ population to $^4I_{13/2}$ states. The data on fluorescence lifetimes and emission cross sections for both transitions are given, and the properties of the stoichiometric hosts for laser applications are discussed. It is concluded that both room-temperature and cooled lasing are possible with different transitions.

TABLE OF CONTENTS


| Section | | Page |
|---|---|---|
| | SUMMARY | 3 |
| | LIST OF ILLUSTRATIONS | 7 |
| 1. | INTRODUCTION | 9 |
| 2. | MATERIALS CONSIDERATIONS | 11 |
| | 2.1 General Considerations | 11 |
| | 2.2 Discussion of Selected Stoichiometric Nd Laser Materials. | 11 |
| 3. | GROWTH OF CRYSTALS OF MOST PROMISING LASER MATERIALS | 15 |
| | 3.1 $NdP_5O_{14}$ (NPP) | 15 |
| | 3.2 $NdLiP_4O_{12}$ (LNP) | 18 |
| | 3.3 $NdAl_3(BO_3)_4$ (NAB) | 21 |
| | 3.4 $Er_xGd_{1-x}P_5O_{14}$ and $Er_xYb_{1-x}P_5O_{14}$ | 24 |
| | 3.5 $Er_xGd_{1-x}LiP_4O_{12}$ and $Er_xYb_{1-x}LiP_4O_{12}$ | 27 |
| | 3.6 $Er_xGd_{1-x}Al_3(BO_3)_4$ and $Er_xYb_{1-x}Al_3(BO_3)_4$ | 29 |
| 4. | OPTICAL PROPERTIES OF STOICHIOMETRIC Nd and Er COMPOUNDS | 32 |
| | 4.1 Spectroscopic Properties of NPP, LNP, and NAB | 32 |
| | 4.2 Flashlamp Pumped NPP Laser | 33 |
| | 4.2.1 Laser Compounds | 33 |
| | 4.2.2 Laser Output Properties | 36 |
| | 4.3 Spectroscopic Properties of $Er_xGd_{1-x}P_5O_{14}$, $Er_xGd_{1-x}LiP_4O_{12}$, and $Er_xGd_{1-x}Al_3(BO_3)_4$ | 41 |
| 5. | CONCLUSIONS | 47 |
| 6. | REFERENCES | 49 |
| | DISTRIBUTION LIST | 51 |

## LIST OF ILLUSTRATIONS


| | | Page |
|---|---|---|
| Fig. 1. | Semi-sealed furnace system for growth of NPP crystals..... | 16 |
| Fig. 2. | Growth temperature vs. fluorescence lifetime for NPP crystals..... | 16 |
| Fig. 3. | Time vs. temperature for growth of NPP crystals..... | 17 |
| Fig. 4. | Crystal of NPP..... | 17 |
| Fig. 5. | Pulling system for top-seeded flux growth of LNP crystals... | 19 |
| Fig. 6. | Single-crystal platelet of LNP grown on surface of flux..... | 19 |
| Fig. 7. | LNP crystal grown by top-seeded flux growth method..... | 20 |
| Fig. 8. | NAB crystals..... | 22 |
| Fig. 9. | Furnace system for top-seeded crystals grown by gradient transport from a fluxed melt..... | 22 |
| Fig. 10. | Effective ionic radii of rare-earth ions as well as minimum growth temperatures and crystal structures of corresponding pentaphosphate crystals of these rare earths..... | 25 |
| Fig. 11. | Crystals of $ErP_5O_{14}$ (scale in mm)..... | 26 |
| Fig. 12. | Crystals of $Er_{0.5}Yb_{0.5}P_5O_{14}$ (10X mag.)..... | 26 |
| Fig. 13. | Crystals of $Er_{0.1}Gd_{0.9}P_5O_{14}$ (scale in mm)..... | 27 |
| Fig. 14. | Crystals of $Er_{0.5}Gd_{0.5}Li(PO_3)_4$ (short prismatic) and $Er_{0.5}Yb_{0.5}Li(PO_3)_4$ (needles)..... | 28 |
| Fig. 15. | Crystals of $YLi(PO_3)_4$ (left) and $Y_{0.8}Gd_{0.1}Er_{0.1}Li(PO_3)_4$ (right)..... | 28 |
| Fig. 16. | $Gd_{0.9}Er_{0.1}LiP_4O_{12}$ crystal as grown on platinum rod..... | 29 |
| Fig. 17. | Large crystal of $GdAl_3(BO_3)_4$ cracked in flux. Small crystal of $Gd_{.994}Er_{.006}Al_3(BO_3)_4$ left intact and clear..... | 30 |
| Fig. 18. | $Gd_{0.7}Er_{0.3}Al_3(BO_3)_4$ crystal grown on platinum rod by top seeding..... | 31 |
| Fig. 19. | Experimental laser setup (SE) and laser head showing pump cavity, flashlamp, and NPP laser rod..... | 34 |

LIST OF ILLUSTRATIONS (Cont'd)


| | | Page |
|---|---|---|
| Fig. 20. | Schematic of flashlamp light discharge circuits with external and series triggering used for experimental laser setup (SE) | 35 |
| Fig. 21. | Hand held laser setup (SHH) and its laser head showing pump cavity (coated with Kodak white reflectance coating 6080) flashlamp, NPP rod, KSF filter, and Q-switch | 35 |
| Fig. 22. | Flashlamp power circuitry for hand-held laser setup (SHH) | 36 |
| Fig. 23. | Output vs. input energy for NPP laser with Type H lamp in experimental setup (SE) | 23 |
| Fig. 24. | Output vs. input energy for NPP laser with Type L lamp in hand-held setup laser head with external power supply | 37 |
| Fig. 25. | Pulse shapes of laser output in Q-switched and free oscillation modes in setups described in Table 5 | 39 |
| Fig. 26. | Typical decay of NPP laser output energy with time at a rate of 5 pps without cooling | 40 |
| Fig. 27. | Transmission spectra of $ErP_5O_{14}$, $LiErP_4O_{12}$, and $ErAl_3(BO_3)_4$ in the visible and near infrared | 42 |
| Fig. 28. | Approximate level diagram of $Er^{3+}$ in $ErP_5O_{14}$, $ErLiP_4O_{12}$, and $ErAl_3(BO_3)_4$ | 43 |
| Fig. 29. | Emission spectra of $ErP_5O_{14}$, $LiErP_4O_{12}$, and $ErAl_3(BO_3)_4$ in eye-safe region | 44 |

## 1. INTRODUCTION

The original goal of this program was the development of a novel laser material for miniaturized laser systems emitting at 1.05 to 1.06 $\mu$m with sufficient energy to satisfy the requirements of existing detectors at a range of at least 2 km.

For miniaturized laser systems, a highly efficient laser material is of primary concern. Until 1975, the Nd-activated material used for solid-state lasers emitting at 1.06 $\mu$m was almost exclusively Nd-YAG. Lasers made from this material, however, were of limited efficiency and could not be miniaturized due to the low maximum permissible doping level of the material (1.0 to 1.5%). Higher doping levels result in substantial non-radiative quenching of the fluorescence in such material. Although significant progress was made over the past several years in preparation of large, high-quality crystals of Nd-YAG, this material does not lend itself to miniaturization since the diameter of the laser rod must be comparable to the absorption length of the pump light to avoid low device efficiency. For the strong pump band centered at 807 nm, the effective absorption length is about 5 mm for conventional Nd-YAG material which is doped to about 1% Nd (at.). Therefore, a side-pumped Nd-YAG laser with a rod diameter much less than 5 mm is quite inefficient (Ref. 1), since the rod diameter is the dominant dimension in determining the level of required pump power and, therefore, the overall size of the device.

In 1973, a new class of unique laser materials came into consideration. These stoichiometric laser materials are pure chemical compounds capable of emitting coherent light in the undiluted state, as opposed to conventional laser materials where the active ions are a "dopant" dispersed randomly in a host. The requirements for such stoichiometric laser material are:

- Be able to grow single crystals that are sufficient in size and stable at ambient temperature.
- The lattice should contain only one type of identical rare-earth sites. The sites should lack a center of inversion, and the distance between sites should be at least 5 Å.
- The gap between the valence and conduction band should be larger than the energy required to pump the four-level laser cycle of the rare-earth ion.

- The crystal should not contain ions which absorb any fluorescence from the rare earth ions.

The first laser material grown within these boundary conditions was $NdP_5O_{14}$, followed by $NdLiP_4O_{12}$, $NdKP_4O_{12}$, and $NdAl_3(BO_3)_4$. Other interesting stoichiometric rare-earth materials are discussed in Section 2 of this report. Many of these compounds containing rare earths other than Nd have never been synthesized or evaluated for their lasing properties. It had been suggested (Ref.2) that the primary consideration in design of a Nd miniature laser is selection of the best active medium among the available high Nd containing materials while the device design should be adapted to the new materials. A survey was therefore made, during the first month of this program, of the luminescence and chemical properties, as well as the synthesis and crystal-growth processes, of all better-known stoichiometric neodymium compounds. $NdP_5O_{15}$, $NdLiP_4O_{12}$, and $NdAl_3(BO_3)_4$ were chosen as the most promising candidates (Sect. 2). Crystals of these materials were grown (Sect. 3), and their luminescent properties were evaluated (Sect. 4) during the following eight months of the program.

During the course of contract review meetings with the Contracting Officer's Technical Representatives on 16 and 29 July 1981, the goals and duration of the program were changed substantially. All technical effort was to be completed by the end of 1981, instead of by 31 October 1982, and was to be concentrated on evaluation of the lasing properties of neodymium pentaphosphate, as well as on the crystal growth and optical evaluation of stoichiometric erbium compounds for miniature lasers emitting in the eye-safe region of the spectrum. This latter effort was a new requirement (Sect. 3 and 4).

## 2. MATERIAL CONSIDERATIONS

### 2.1 General Considerations

Table 1 lists the better known stoichiometric Nd compounds, together with their acronyms and some important crystallographic data, which fulfill the basic requirements for stoichiometric rare-earth compounds suitable for miniature laser applications. Other properties of the compounds which have to be considered for their practical use in miniature lasers are their fluorescence properties such as effective cross section, lifetime, and pump threshold (see Table 2).

Pertaining to stoichiometric erbium compounds, little is known about their crystal growth or lasing properties. We decided, however, to use the same techniques best known to us for the growth of stoichiometric Nd-compounds to grow Er compounds and to concentrate on the growth of $ErP_5O_{14}$, $ErLiP_4O_{12}$, and $ErAl_3(BO_3)_4$, with and without the addition of Yb or Gd for energy transfer and/or dilution purposes.

### 2.2 Discussion of Selected Stoichiometric Nd Laser Materials

$NdP_5O_{14}$ (NdPP) has, next to KNLF and LNP, the highest lifetime; most progress in high concentration mini-lasers has been with this material. In the past, we had grown large crystals of this material and fabricated mini-laser rods from them (Ref. 3). One minor disadvantage of these crystals is their tendency to cleave easily in the (010) plane. As a result, laser rods of this material have to be fabricated with a square or rectangular cross section rather than a round one. The crystals appear to be stable in high humidity atmospheres and at elevated temperatures at least up to their $P2_1/C$ --> Pncm phase transition which occurs at 115°C.

$NdLiP_4O_{12}$ (LNP) is similar to NdPP in its coordination, fluoresence, and lasing properties. It does not have the cleavage problem, however, and fabrication of round laser rods may be feasible. LNP could be equal or slightly superior to NdPP in device performance, but any advantage may be outweighed by the fact that large clear crystals are far more difficult to grow as those of NdPP.

TABLE 1: Comparison of crystallographic data of stoichiometric Nd compounds.

| Compound | Acronym | Crystal System | Space Group | Unit Cell | Nd Coord. | Nearest Nd-Nd Distance (Å) | Nd Conc. ($10^{21}$ $cm^{-3}$) |
|---|---|---|---|---|---|---|---|
| $NdO_5O_{14}$ | NPP | monocl. | $P2_1/c$ | 4 | 8 | 5.19 | 3.96 |
| $NdLiP_4O_{12}$ | LNP | monocl. | C2/c | 4 | 8 | 5.62 | 4.37 |
| $NdKP_4O_{12}$ | KNP | monocl. | $P2_1$ | 2 | 8 | 6.66 | 4.08 |
| $NdAl_3(BO_3)_4$ | NAB | trig. | (R32) | 3 | 6 | 5.92 | 5.43 |
| $NdK_5(MoO_4)_4$ | NKM | trig. | $R\bar{3}m$ | 1.5 | 6 | 5.98 | 2.32 |
| $NdNa_5(WO_4)_4$ | NST | tetrag. | $I4_1/a$ | 1.5 | 8 | 6.02 | 2.6 |
| $K_5NdLi_2F_{10}$ | KNLF | hexag. | Pnma | 4 | 8 | 6.73 | 3.6 |

TABLE 2: Effective cross section $\sigma_E$, fluorescence lifetime $\tau$ and lowest observed pump threshold $A_T$ for $4F_{3/2} \dashrightarrow 4I_{11/2}$ transition of stoichiometric Nd compounds.

| Material | Nd Site Symmetry | $\sigma_E$ ($10^{-19}$ $cm^2$) | $\tau$ ($\mu s$) | $A_T$ (mW) |
|---|---|---|---|---|
| $NdP_5O_{14}$ | 1 | 2 | 135 | 0.45 |
| $NdLiP_4O_{12}$ | 2 | 3.2 | 135 | 0.20 |
| $NdKP_4O_{12}$ | 1 | ~1.5 | 100 | 0.45 |
| $NdAl_3(BO_3)_4$ | ~32 | 10 | 20 | 0.55 |
| $NdK_5(MoO_4)_4$ | $(\bar{3}m)$,1 | 0.7 | 60 | 15 |
| $NdNa_5(WO_4)_4$ | $\bar{4}$ | ~7 | 85 | 0.33 |
| $K_5NdLi_2F_{10}$ | | 0.8 | 300 | 1.4 |

$NdKP_4O_{12}$ (KNP) is similar to LNP but has a slightly shorter fluorescence lifetime. Another important difference is that KNP has an acentric space group which, in principle, allows both linear electro-optic modulation and second-order nonlinear optical effects. Unfortunately, it seems that these effects are too small to permit frequency doubling on a practical scale. Clear crystals of larger size are equally difficult to grow as those of LNP.

$NdAl_3(BO_3)_4$ (NAB) was the first non-phosphate stoichiometric Nd-laser material to be developed. In contrast to the phosphates, the Nd-O coordination is only six-fold, resulting in a substantial deviation from inversion symmetry. The resulting large odd-parity f-d admixture makes the lifetime appreciably shorter. There is, however, a corresponding increase in emission cross section. Like KNP, NAB has an acentric square group. Measurements performed by us on NAB gave a second-harmonic signal with an intensity of only 0.2 of that of quartz. The signal increased in intensity to twice that of quartz with addition of yttrium to NAB. This can be explained by the fact that pure NAB shows alternating domains consisting of a C2 and C2/c phase, which are both subgroups of C2/m (Ref. 4). Addition of yttrium, however, seems to force NAB to crystallize in a single phase.

$NdK_5(MoO_4)_4$ (NKM) does not exactly belong into this new class of laser materials since there is a statistical 1:1 $K^+$,$Nd^{3+}$ occupancy of the rare-earth sites. In fact, the material would not lase without this statistical distribution. Crystals have a relatively narrow cross section and a high pump threshold. In addition, there are severe thermal problems with this material due to very poor thermal conductivity, and the material is not stable in moist air.

$NdNa_5(WO_4)_4$ (NST) may also have a statistical distribution for Nd + Na. However, its large cross section, low threshold, and strong absorption compares favorably with those of the phosphate compound. Unfortunately, the growth of even small optically clear crystals is very difficult, and NST offers therefore no advantage over the phosphates.

$K_5NdLi_2F_{10}$ (KNLF) is a recently discovered laser material with a very long fluorescence lifetime. However, its use is limited since the crystals are said to be water soluble and hygroscopic.

In summary, NdPP and LNP appear to be the most promising candidates for miniature lasers. Although crystals of NAB are very difficult to grow, their fluoresence properties justified an attempt to produce crystals large enough in size to permit optical evaluation studies.

## 3. GROWTH OF CRYSTALS OF MOST PROMISING Nd LASER MATERIALS

### 3.1 $NdP_5O_{14}$ (NPP)

$NdP_5O_{14}$ does not melt congruently but decomposes before melting at 1400°C. Crystal are grown from a seed in a phosphoric acid flux inside a semi-sealed furnace system (see Fig. 1). A technique for growing crystals of up to 3 cm in diameter, previously developed by us, is described in the literature (Ref. 3). We have established that a specific temperature profile inside the flux and a precisely controlled evaporation rate of $H_2O$ produced during growth are essential.

Since the lifetime of the $Nd^{3+}$ $4F_{3/2}$ fluorescence increases significantly with increasing growth temperature (Fig. 2) for NPP crystals, we studied this influence and determined, at the same time, the optimum, i.e., the maximum, permissible growth temperature. In our semi-sealed growth system (Ref. 3), two major factors determine the upper temperature limit for growth of NPP, viz., vapor pressure of the acid mixture and thermal stability of the vitreous carbon crucible. Too high a temperature and therefore too-high a vapor pressure leads to: severe losses of $P_2O_5$ ($+H_2O$) and thereby multiple nucleation, poor-quality crystals, severe chemical attack of all quartz parts of the system, and severe thermal attack (oxidation) of the carbon crucible. In our system, there is a narrow temperature range in which crystals of NPP with a maximum fluorescence lifetime can be grown without reaching such conditions; this temperature range was determined to be between 550 and 590°C. Figure 3 shows the time and temperature for a NPP growth run under such "optimum" conditions. Laser rods 2 x 2 x 20 mm were fabricated from crystals produced under such conditions (Fig. 4). The crystals were up to 35 mm in cross section and of high optical quality.

Fabrication of laser rods from NPP crystals is known to be difficult (Ref. 3) The main problem is "scaling" of the "b" face during final cutting of the laser rods from plates having optically polished "c" faces. The scaling is particularly noticeable toward the edges. In addition, we observed, occasionally, cleavage cracks in the rods parallel to the "c" end faces, which developed during final cutting. We believe the cracks formed during polishing of the end faces and were caused by movement of the ferroelastic domain walls which are parallel to the "c" face.

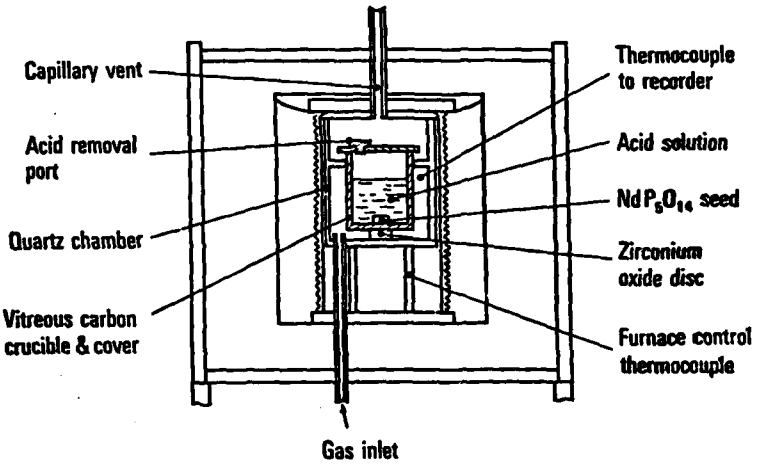


Figure 1. Semi-sealed furnace system for growth of NPP crystals.

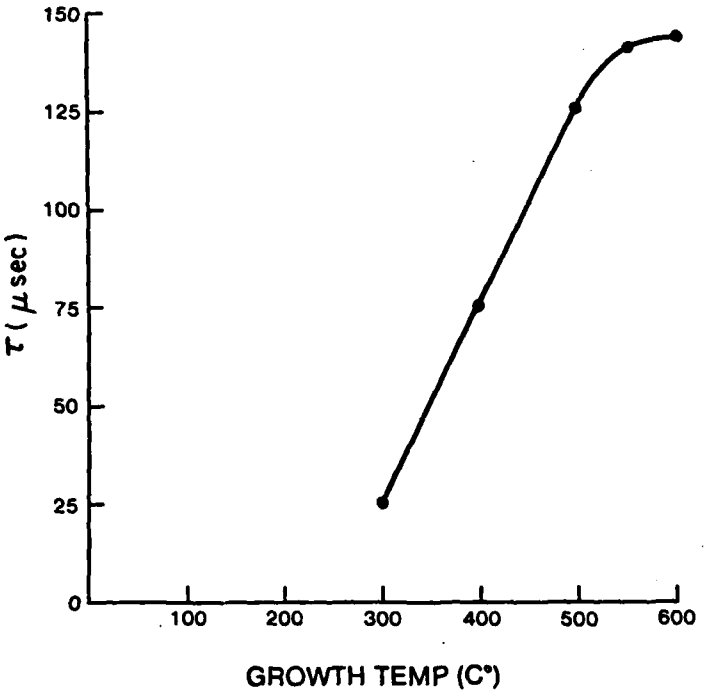


Figure 2. Growth temperature vs. fluorescence lifetime for NPP crystals.

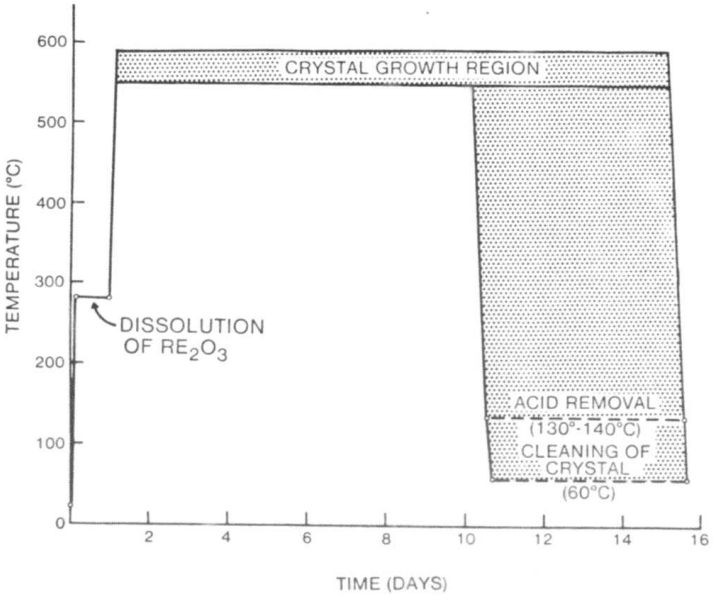


Figure 3. Time vs. temperature for growth of NPP crystals.

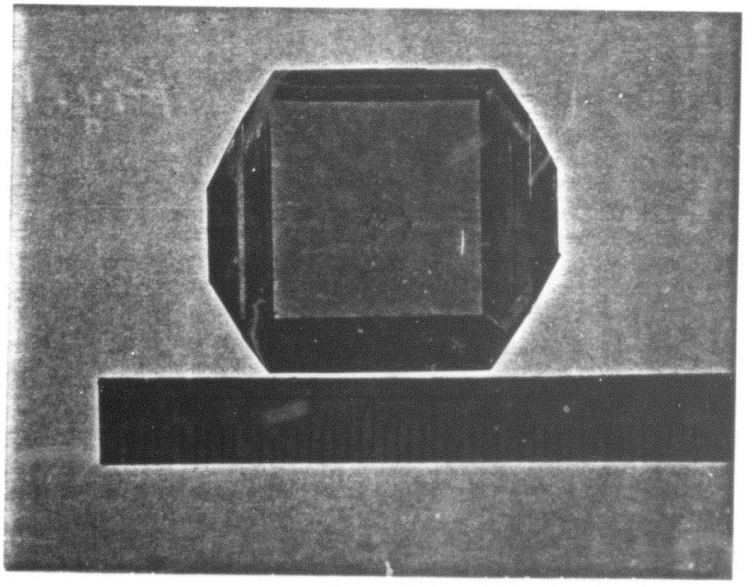

Figure 4. Crystal of NPP.

## 3.2 $NdLiP_4O_{12}$ (LNP)

$NdLiP_4O_{12}$ also melts incongruently, i.e., it disassociates at 970°C. Crystal-growth techniques used for this material are either flux growth or the Kyropoulos technique (top seeding). Starting materials are $Li_2CO_3$, $Nd_2O_3$, and $NH_4H_2PO_4$ which decompose during premelting of the mixture to a flux consisting essentially of $LiPO_3$, $Li_4P_2O_7$ and $P_2O_5$ from which LNP crystallizes during cooling. Composition of the flux can influence, of course, the growth and quality of the crystals. We studied the $P_2O_5$ - $Li_2O$ - $Nd_2O_3$ phase diagram to optimize flux composition and, thereby, the growth. Since the growth was performed below 950°C, Kanthal resistance furnaces were used; several three-zone furnace systems were set up for the growth. Since top-seeded growth requires a very slow pull rate, we purchased and set up a crystal puller permitting pulling rates of less than 100 $\mu$m per hour (Fig. 5).

The molar ratios of the oxides $Li_2O$:$Nd_2O_3$:$P_2O_5$ were varied between 40-44:1-5:50-53. Attempts were made to grow crystals by slow cooling of these melts at rates ranging from 0.5 - 2°C/hour. Slow cooling rates and low $Nd_2O_3$ concentrations produced the best results. Since the melt tends to supersaturate, the crystallization occurs spontaneously at a certain point, resulting in poor-quality crystalline aggregates. Although lower $Nd_2O_3$ concentrations seem to minimize this effect, crystals inside the flux were of poor quality.

The only crystals of good optical quality grew on top of the melt in the form of platelets up to about 0.5 x 5 x 10 mm (see Fig. 6). The platelets were used for optical evaluation studies (see Section 4). The results indicate that the system lends itself well for top-seeded growth.

The purchased crystal puller was modified and equipped with a linear displacement transducer which not only enabled the measurement and recording of the stability of the pulling rate but also precise repositioning of the seed within $\pm$ 2 $\mu$m. Rotation of the seed was varied between 10 and 60 rpm. The composition of the fluxed melt in our preliminary growth experiments in mol ratios for $LiO_2$:$Nd_2O_3$:$P_2O_5$ was 3:1:6. The temperature at the

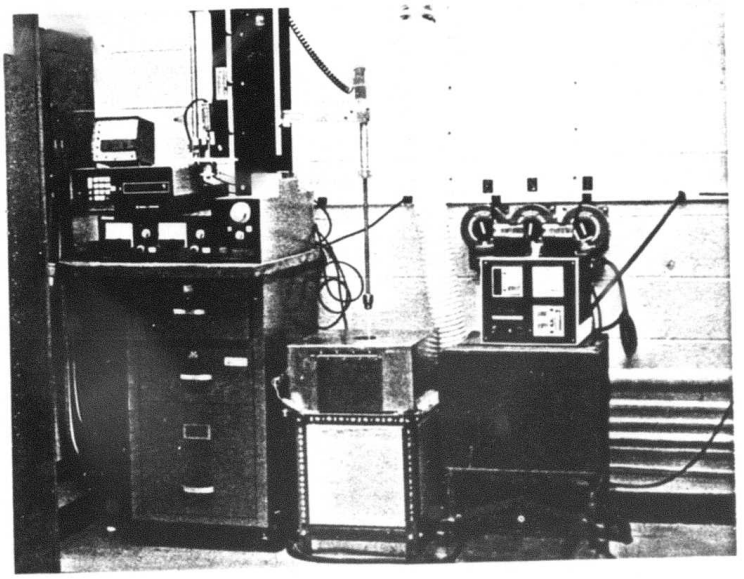

Figure 5. Pulling system for top-seeded flux growth of LNP crystals.

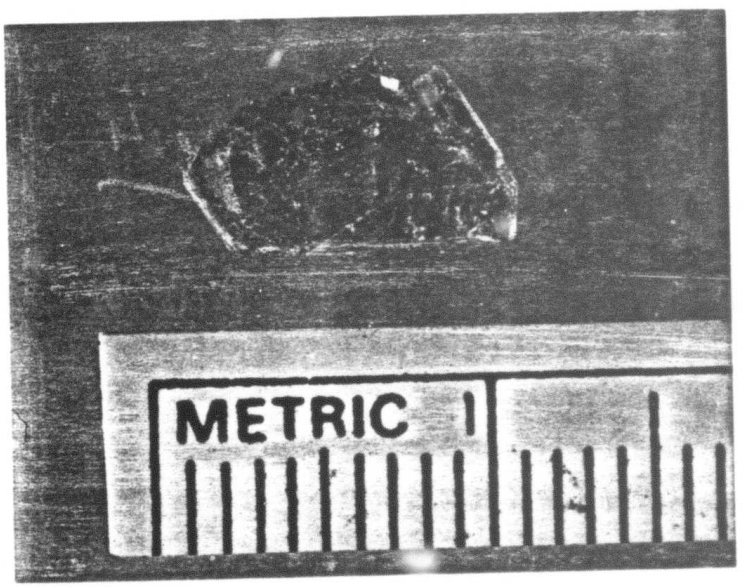


Figure 6. Single-crystal platelet of LNP grown on surface of flux.

melt surface was varied between 870°C and 950°C, and the temperature gradient between the surface and bottom of the melt was between 1°C and 5°C while the pulling rate was varied between 80 and 150 $\mu$m/hr.

Figure 7 is a photograph of an LNP crystal ($\sim$1 cm in diameter) pulled under such conditions by top seeding. Growth rate in the b-direction of LNP crystals is about twice as fast as in the other directions; crystals grown in this direction are of the best quality. Major difficulties are inclusions in the crystals as well as multiple nucleation.

In summary, the Kyropoulos technique appears to be the best method for the growth of larger crystals of LNP. It is questionable, however, whether this technique lends itself to production, on a routine basis, of crystals 2 cm in length, for miniature laser rods. In addition, it would appear to be even more difficult to produce such large crystals which are free of minor inclusions that would generate light scattering during lasing.

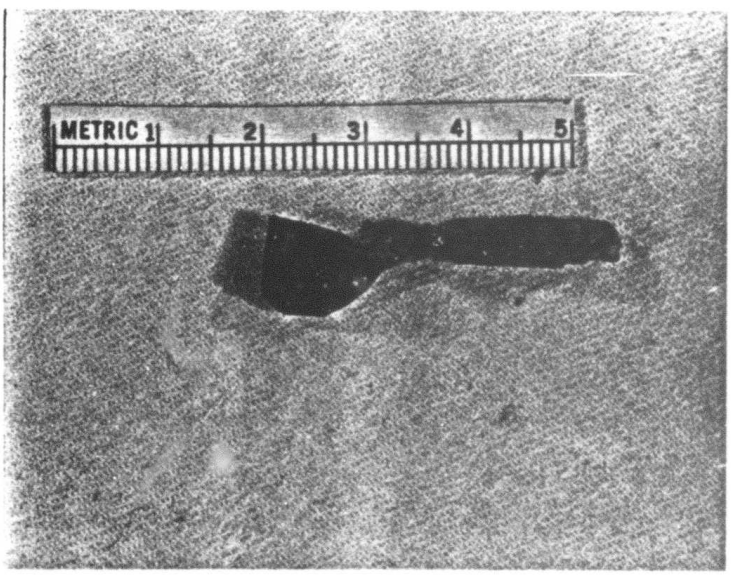


Figure 7. LNP crystal grown by top-seeded flux growth method.

### 3.3 $NdAl_3(BO_3)_4$ (NAB)

This compound also decomposes prior to melting at 1220°C, and crystals have to be grown, therefore, from fluxed melts such as $Li_2O:B_2O_3$, $K_2O:3MoO_3$, $BaO::B_2O_3$, $PbO:B_2O_3$, $PbF_2:B_2O_3$ or $Bi_2O_3:B_2O_3$ to which $Nd_2O_3$, $Al_2O_3$ and $B_2O_3$ had been added. However, the addition of other foreign and optically inactive ions, e.g., $Gd^{3+}$, is necessary to obtain a crystallographically single phase of this compound. Since these fluxes have a much higher melting point than the ones used for LNP, we constructed and set up three single and one three-zone platinum furnace systems. Similar to LNP, it is believed that top seeding techniques would produce better quality crystals than crystals grown at the bottom of the crucible.

Table 3 summarizes the exploratory experiments with NAB. The first experiment at 1020°C (melt #1) produced crystals of $NdAl_3(BO_3)_4$ up to 1 cm in

TABLE 3: List of Exploratory Experiments with NAB.

| Melt No. | Crystal | Flux |
|---|---|---|
| 1 | $NdAl_3(BO_3)_4$ | $PbF_2:B_2O_3$ |
| 2 | $NdAl_3(BO_3)_4$ | $Bi_2O_3:B_2O_3$ |
| 3 | $NdAl_3(BO_3)_4$ | $BaO:BaF_2:B_2O_3$ |
| 4 | $Nd_{0.33}Y_{0.67}Al_3(BO_3)_4$ | $PbO:B_2O_3$ |
| 5 | $Nd_{0.67}Y_{0.33}Al_3(BO_3)_4$ | $PbO:B_2O_3$ |
| 6 | $NdAl_3(BO_3)_4$ | $PbO:B_2O_3$ |

size (see Fig. 8). The crystals were not optically clear, however, which may be partially due to flux inclusions and partially due to the presence of two phases. In addition, some top seeding experiments were performed using gradient transport of material from the bottom of the crucible (see Fig. 9), although the $PbF_2$ was too volatile for this work. The real problem was the two-phase nature of the crystals as seen by X-ray diffraction. This is similar to that reported by Jarchow et al. [Ref. 5] who showed that their crystals of $NdAl_3(BO_3)_4$ had C2/c and C2 phases. It is possible that their crystals contained Nd aluminum dimetaborate, a P6/mmm class material as reported by D. Yu. Pushchrovskii et al. [Ref. 6]. This phase is obtained

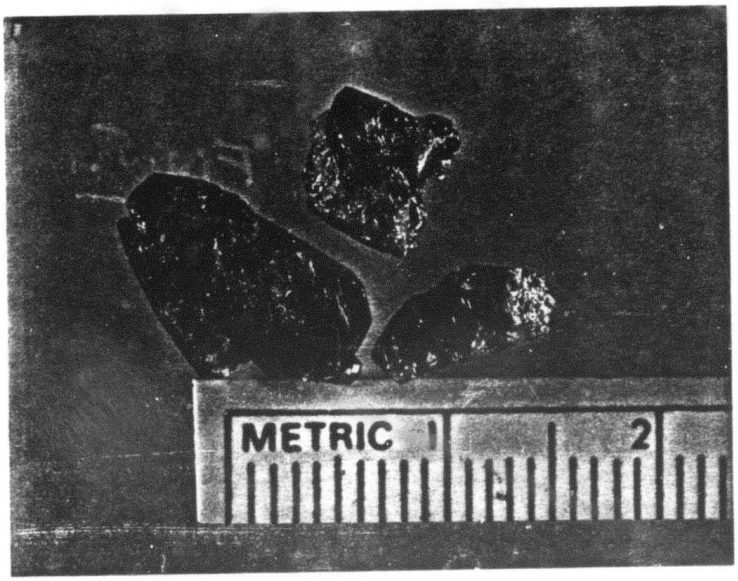


Figure 8. NAB crystals.

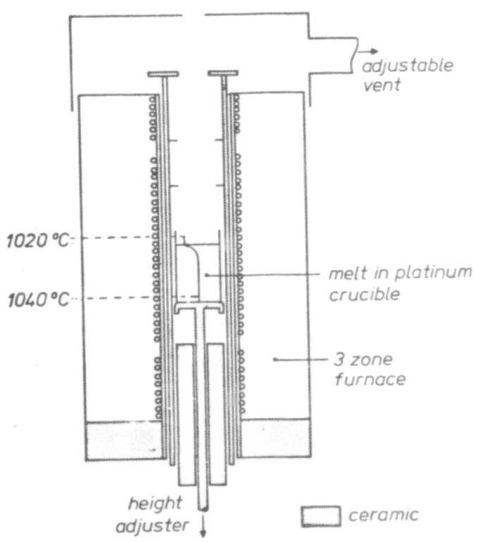


Figure 9. Furnace system for top-seeded crystals grown by gradient transport from a fluxed melt.

when the supersaturation is too high. The other problem was that this melt composition produced a second phase as well as the crystals. This phase, now identified as $9Al_2O_3$, $2B_2O_3$, was formed by too-high a $B_2O_3$ content in the melt or too high a $NdAl_3(BO_3)_4$ concentration. This may also be a clue to the two-phase nature of the crystals if this aluminum borate grows into the crystals.

The lifetime of these NAB crystals grown from the $PbF_2$ flux was found to be 16 $\mu$s (see Sect. 4); this is in very good agreement with the literature [Ref. 7].

A melt using $Bi_2O_3$ (melt #2 Table 3) was used in another attempt to grow $NdAl_3(BO_3)_4$. It was assumed that if such a growth were successful, it would be interesting from two points of view. The simultaneous incorporation of the $Bi^{3+}$ ion can act as a sensitizer as, for example, in the case of $TbAl_3(BO_3)_4$ [Ref. 8], and also this ion would be the largest that could possibly be substituted for the RE. Until now, only RE gallium [Ref. 9] and RE iron borates [Refs. 10,11] have been grown from this flux system, and not the aluminum borates. Using melt composition #2, crystal growth was attempted between 1100 and 950°C. The growth was unsuccessful and may be due to the low solubility of the $NdAl_3(BO_3)_4$ in this melt or that the growth does not work for aluminum borates.

With the melt composition based on $BaO:BaF_2:B_2O_3$ (#3), an attempt was made to grow $NdAl_3(BO_3)_4$ and to top seed the melt. This run did not produce any crystals. One result was clear from this experiment, viz., there was little evaporation and virtually no attack of the alumina furnace tubes; thus, the expensive platinum liners may not be necessary.

The last three exploratory experiments were based on the $PbO/B_2O_3$ flux combination. The reasons for doing these experiments were: a) the evaporation rate is not too high, thus top-seeding could be attempted, b) the flux produces large crystals of good quality. A remark made by a Russian conferee at the 1980 ICCG-6 conference in Moscow suggested that the Nd-Y system would produce a better laser crystal than that from the system containing only Nd. Three melts were therefore made in which the Nd/Y mole ratio was 1/3, 2/3 and pure Nd. A parallel experiment reported by Leonyuk et al.

[Ref. 12] using a $K_2O.3MoO_3$ flux showed that up to 72 mole % substitution of yttrium by neodymium was good. At higher concentrations, molybdates were formed. It should be noted that two other publications by the same authors [Refs. 13,14] reported that they were able to produce the pure $NdAl_3(BO_3)_4$ from the $K_2O.3MoO_3$ flux.

Melt #4 produced crystals on the bottom of the crucible. No second phases were found, and the lifetime was measured to be 40-60 $\mu$s with 33% Nd depending on which crystal was used. Melt #5 produced some crystals and a polycrystalline mass. The lifetime was measured to be 34 $\pm$ 3 $\mu$s with 67% Nd. Finally, melt #6 did not produce any crystals, only flakes in the melt. One point was clear, viz., mixed crystals produce lifetimes which are better for laser applications.

In summary, our studies of the NAB crystals indicate that it would be extremely difficult to grow single crystals of good optical quality and large enough for fabrication of laser rods. Recent studies by other workers of the crystal structure of NAB produced contradictory results with respect to the single or multiple-phase nature of these crystals. We, therefore, discontinued our crystal growth experiments on NAB in the early stages of the program.

### 3.4 $Er_xGd_{1-x}P_5O_{14}$ and $Er_xYb_{1-x}P_5O_{14}$

Crystals of compounds of both of these series were grown by basically the same technique described in Section 3.1 for the growth of NPP crystals (Ref. 3). However, since growth temperature, solubility, and even crystal structure of the resulting product will change with changing effective radius of the rare earth ions (see Fig. 10), optimum growth conditions have to be established for each individual compound.

$ErP_5O_{14}$ crystals required a solution about three times as concentrated as that for NPP crystals (i.e., a mass fraction of ~10% instead of 3.5% of RE oxide). The growth temperature was 680°C, which is about 100°C higher than the growth temperature for NPP crystals. The resulting crystals were

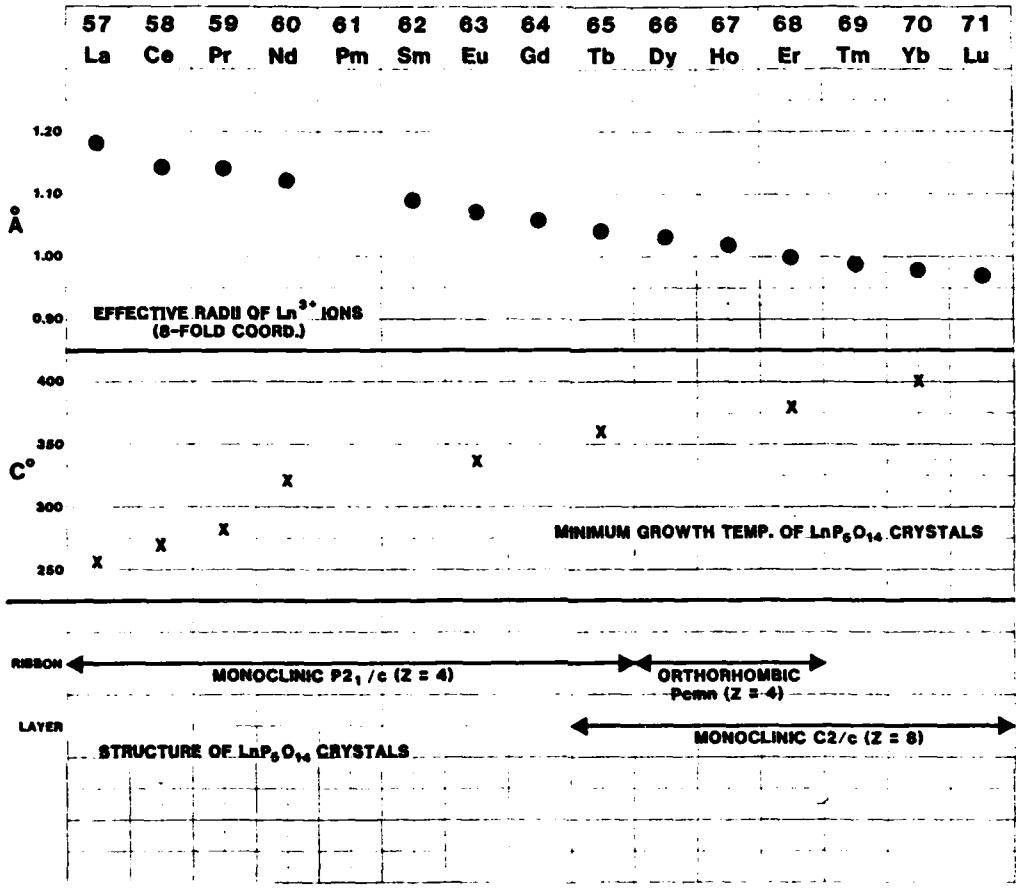


Figure 10. Effective ionic radii of rare-earth ions as well as minimum growth temperatures and crystal structures of corresponding pentaphosphate crystals of these rare earths.

mostly prismatic or hexagonal shaped and averaged about 1 x 2 x 3 mm (see Fig. 11).

$Er_{0.5}Yb_{0.5}P_5O_{14}$ crystals, grown under identical conditions, were of similar shape, with an average size of 2 x 2 x 5 mm but not free of some inclusions (see Fig. 12).

$Er_xGd_{1-x}P_5O_{14}$ crystals with x of 0, 0.1, 0.3, 0.5 and 0.7 were all grown, again, under similar conditions. The crystals were prismatic or hexagonal-shaped, and up to 2 x 2 x 5 mm in size. Many contained inclusions in their centers. Up to 1 cm large clear crystals of $Er_{0.1}Gd_{0.9}P_5O_{14}$ (Fig.13) were

produced from small seeds of this material. This composition was chosen because of the theoretical considerations discussed in Section 4 of this report.

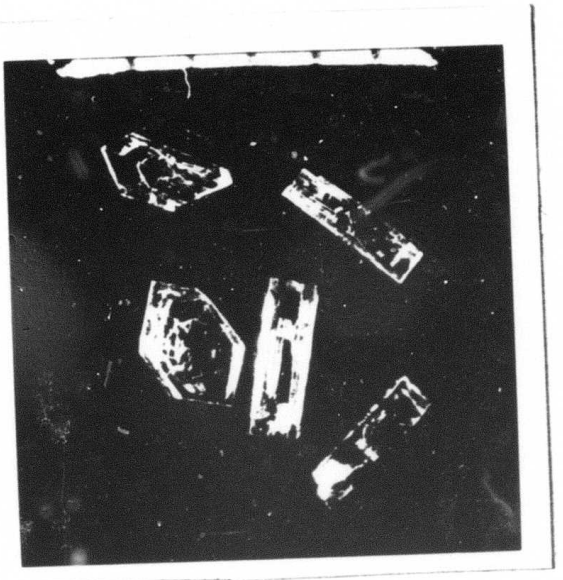

Figure 11. Crystals of $ErP_5O_{14}$ (scale in mm).

Figure 12. Crystals of $Er_{0.5}Yb_{0.5}P_5O_{14}$ (10X mag.).

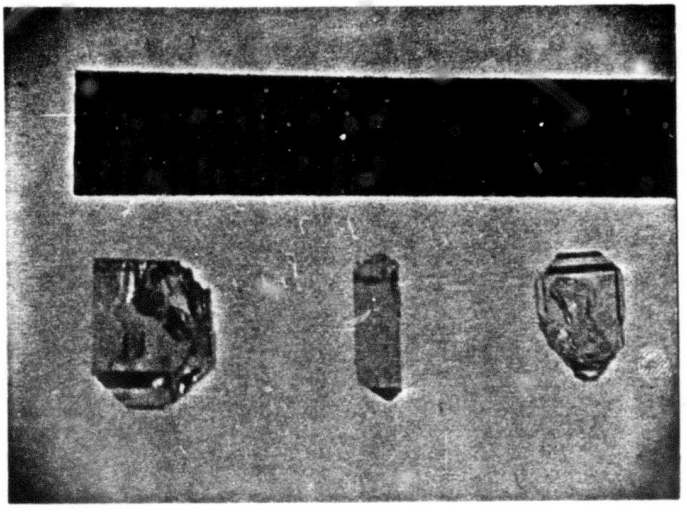

Figure 13. Crystals of $Er_{0.1}Gd_{0.9}P_5O_{14}$ (scale in mm).

### 3.5 $Er_xGd_{1-x}LiP_4O_{12}$ and $Er_xYb_{1-x}LiP_4O_{12}$

A series of crystal growth runs was made using fluxed melts of $Li_2O$ and $P_2O_5$ in which the rare earth oxides were dissolved. The flux was held at 800°C for 16 hours and cooled 1°/hour to 700°C. The run was then air-quenched to 500°C and cooled in a furnace at 100°C/hour to room temperature. These runs were similar to the flux growth runs for LNP.

Erbium or ytterbium and erbium-containing crystals tended to be needle-like while gadolinium and erbium-containing crystals tended to show a short prismatic morphology. All of these crystals suffered from a bubble-like feature on the surface (see Fig. 14) which may be due to the flux-dissolving back material. In addition, most of the crystals had various types of inclusions.

Growth experiments were also performed on $YLiP_4O_{12}$ (LYT), a possible new laser host. Very clear platelets of $YLiP_4O_{12}$ (Fig. 15, left) and $Y_{0.8}Gd_{0.1}Er_{0.1}LiP_4O_{12}$ (Fig. 15, right) were grown. These preliminary experiments showed that, under the same growth condition, LYT with erbium and gadolinium produces crystals of better optical quality.

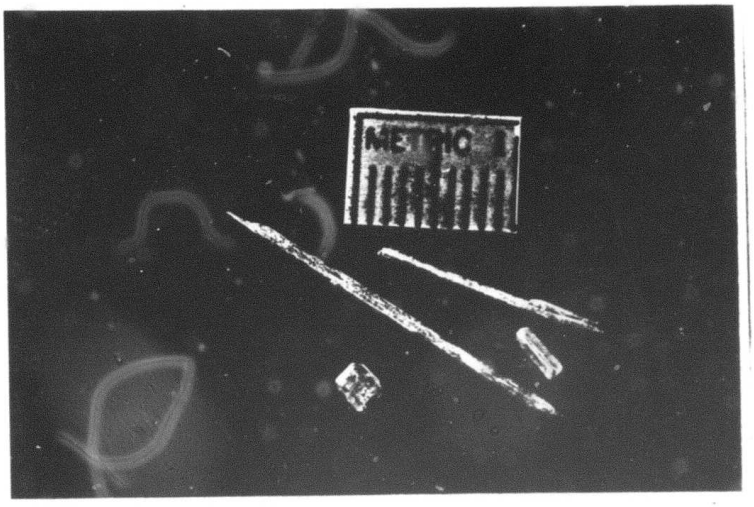

Figure 14. Crystals of $Er_{0.5}Gd_{0.5}Li(PO_3)_4$ (short prismatic) and $Er_{0.5}Yb_{0.5}Li(PO_3)_4$ (needles).

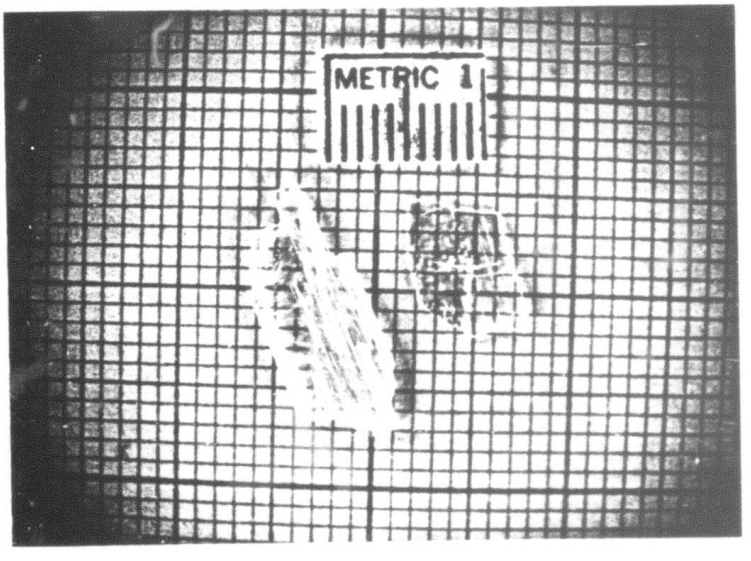


Figure 15. Crystals of $YLi(PO_3)_4$ (left) and $Y_{0.8}Gd_{0.1}Er_{0.1}Li(PO_3)_4$ (right).

$Gd_{0.9}Er_{0.1}LiP_4O_{12}$ crystals were also grown by top seeding a fluxed melt containing the following mol/ratios: $Gd_2O_3$ (0.9), $Er_2O_3$ (0.1), $Li_2O$ (3.0), $P_2O_5$ (6.0). Cooling rates of this melt were 0.1 to 1°C per hour, and the seed was rotated 1-5 rpm without pulling (see Fig. 16).

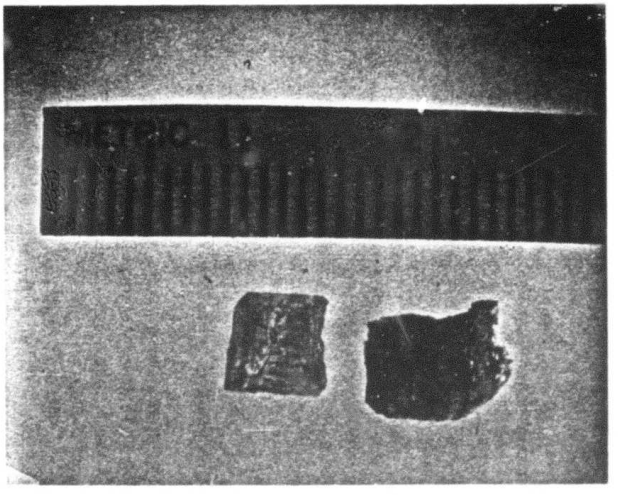

Figure 16. $Gd_{0.9}Er_{0.1}LiP_4O_{12}$ crystal as grown on platinum rod.

3.6 $Er_xYb_{1-x}Al_3(BO_3)_4$ and $Er_xGd_{1-x}Al_3(BO_3)_4$

Crystals of these compounds were grown by a fluxed melt technique described previously (Ref. 15) for the growth of NAB crystals. The composition of the melt was:

76.32 g PbO
95.52 g $B_2O_3$
10.65 g $Gd_2O_3$ or $Yb_2O_3$
21.82 g $Al_2O_3$
16.85 g $Er_2O_3$

Although the crystals were up to 15 mm in cross section, they contained very few clear areas. Preliminary experiments on the growth of such crystals from a $Li_2O$-$B_2O_3$ flux were unsuccessful since the flux did not clear even at elevated temperatures.

The best crystals of $Er_xGd_{1-x}Al_3(BO_3)_4$ with x between 0.005 and 0.95 were grown in a series of runs from a fluxed melt produced from:

| | |
|---|---|
| $(Er,Gd)_2O_3$ | 8 g |
| BaO | 7.5 g |
| $Al_2O_3$ | 7.5 g |
| $B_2O_3$ | 15 g |

The charge was heated to 1250°C for 5 hours and subsequently cooled to 1200°C. After the melt stabilized for another 5 hours, it was cooled at a rate of 1°C per hour to 1100°C and from thereon to room temperature at 50°C per hour. The crystals were large (up to 20 mm x 5 mm x 3 mm) and clear. The flux, however, contracted so much on cooling that the crystals cracked (see Fig. 17).

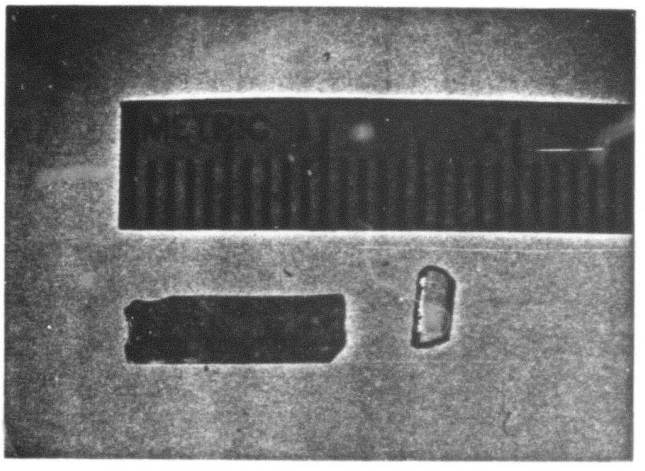

Figure 17. Large crystal of $GdAl_3(BO_3)_4$ cracked in flux. Small crystal of $Gd_{.994}Er_{.006}Al_3(BO_3)_4$ left intact and clear.

Growth of crystals of $Gd_{0.7}Er_{0.3}Al_3(BO_3)_4$ was also attempted by the flux pulling method from a platinum rod with seed holder without cooling, but only a temperature gradient in the melt. Clear rods up to 5 mm x 3 mm x 2 mm were produced (see Fig. 18).

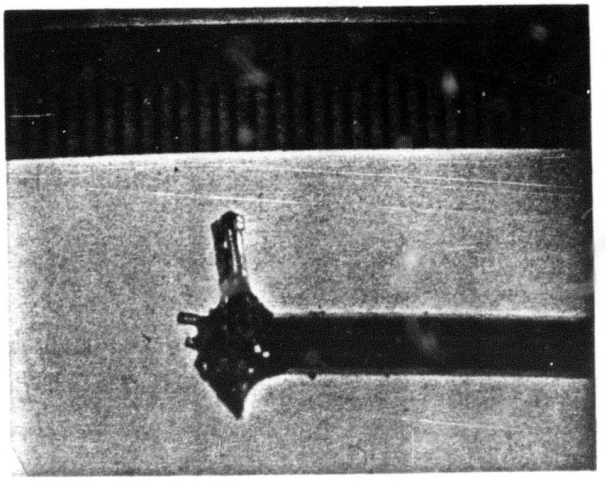

Figure 18. $Gd_{0.7}Er_{0.3}Al_3(BO_3)_4$ crystal grown on platinum rod by top seeding.

## 4. OPTICAL PROPERTIES OF STOICHIOMETRIC Nd AND Er COMPOUNDS

### 4.1 Spectroscopic Properties of NPP, LNP, and NAB

The spectroscopic properties of NPP, LNP, and NAB crystals were studied with the techniques and setups described earlier (Ref. 16). The experimental studies gave the $^4F_{3/2}$ fluorescence lifetime and $^4F_{3/2} \rightarrow {}^4I_{11/2}$ emission cross sections of $Nd^{3+}$ in these stoichiometric materials grown by us. These results for all three crystal types are summarized in Table 4, together with calculated data on the expected threshold energy and typical output energies. The values in parenthesis are the data collected by G. Huber (Ref. 7) on the same type materials (see also Table 2).

In addition to the parameters listed in Table 6, absorption and emission spectra of all these three materials were studied (Refs. 15,17). The results of these studies agree with the well established absorption and emission properties of NPP, LNP, and NAB. As seen from Table 4, all of the three crystal types give similar laser properties of $Nd^{3+}$. Because of this similarity and the availability of large-size crystals of NPP, the experimental laser studies were done only with NPP rods.

TABLE 4. Laser Properties of NPP, LNP, and NAB.

| Crystal | $\tau$ | $\sigma_e$ | $(\sigma_e\tau)^{-1}$ | $E_T$ | $E_{out}$ |
|---|---|---|---|---|---|
| NPP | 140 | $2.4\times10^{-19}$ | $3.0\times10^{22}$ | 0.42 | 33 |
| | (120) | ($2\times10^{-19}$) | ($4.2\times10^{22}$) | | |
| LNP | 140 | $2.5\times10^{-19}$ | $2.9\times10^{22}$ | 0.40 | 34 |
| | (120) | ($3.2\times10^{-19}$) | ($2.6\times10^{22}$) | | |
| NAB | 16 | $6.5\times10^{-19}$ | $9.6\times10^{22}$ | 1.40 | 24 |
| | (20) | ($10\times10^{-19}$) | ($5\times10^{22}$) | | |

$\tau$ = Fluorescence lifetime of $^4F_{3/2} \rightarrow {}^4I_{11/2}$ line ($\mu$s).

$\sigma_e$ = Emission cross section of $^4F_{3/2} \rightarrow {}^4I_{11/2}$ line ($cm^2$).

$(\sigma_e\tau)^{-1}$ = Threshold parameter $(sec\text{-}cm^2)^{-1}$ [see Ref. 16].

$E_T$ = Threshold energy for pulsed operation (J) assuming 2% pumping efficiency, 65% output coupling, 2% internal loss, 2x2 mm crystal area, and 80 $\mu$s pump pulse.

$E_{out}$ = Output energy for 4 J electrical input energy (J). Parameters are same as for $E_T$.

## 4.2 Flashlamp Pumped NPP Lasers

### 4.2.1 Laser Components

The laser setups used in these studies were mainly of two types, viz., an experimental setup (Type SE) and a hand-held setup (Type SHH). With the experimental setup (see Fig. 19), it was relatively easy to change the various components of the laser cavity, and the flashlamps were fired with either series or external triggering (see Fig. 20). In the hand-held setup (see Fig. 21), a KSF UV filter (Kigre Inc.) and a passive Q-switch material (Eastman Kodak 15064) were built in. The main power circuitry for this setup (see Fig. 22) used external triggering and was designed for single-pulse operation. For high energy pulses, the laser head of this SHH setup was also used with the triggering circuitry shown in Figure 20.

The laser pump cavities used in the laser setups were either elliptical or circular. However, most of the results presented here are with circular or nearly circular pump cavities with a diameter of about 7-8 mm. The cavities were made of either brass or glass, and the reflecting surfaces were coated with either silver, aluminum, or BaS (Kodak 6080). The use of different cavities with different coatings did not cause any observable changes in the output of the lasers.

The NPP laser rods were pumped by mainly two types of linear Xe flashlamps. The first type (Type L) had a large diameter (3.6 mm O.D.) (Siemens CG2220, or similar) and could go to high electrical energies but with low efficiency. The second type (Type H) had a smaller diameter (2.4 mm O.D.) (GTE Sylvania, or similar) and operated at energies up to 8 J with higher pumping efficiency than that of the Type L flashlamp. The Type H flashlamp had fill pressures between 450-1200 Torr. The laser output behavior showed no considerable change with different-pressure Type H lamps. The fill pressures for the Type L lamps were not specified, but from pumping efficiency and triggering properties, it was estimated to be lower than 400 Torr. Pertaining to the results presented in this report, the lamps used had arc lengths of about 20 mm.

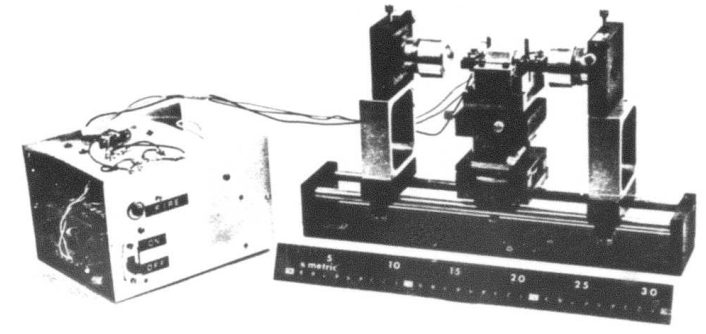


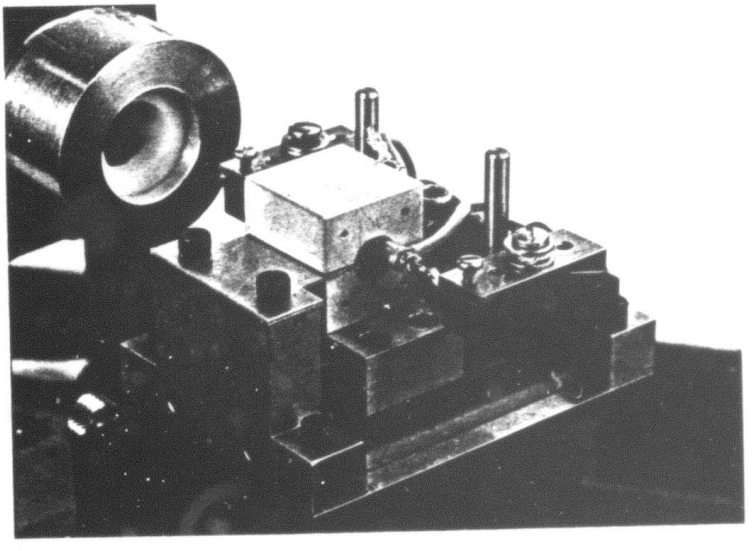

Figure 19. Experimental laser setup (SE) and laser head showing pump cavity, flashlamp, and NPP laser rod.

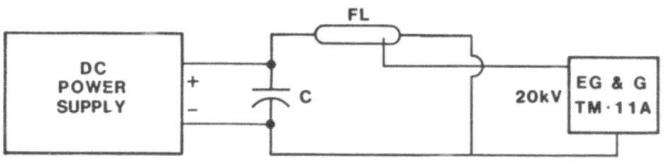


(a) External Triggering.

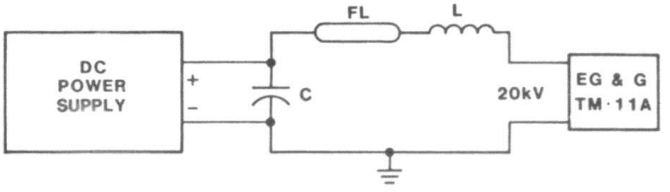


(b) Series Triggering.

Figure 20. Schematic of flashlamp discharge circuits with external and series triggering used for experimental laser setup (SE).

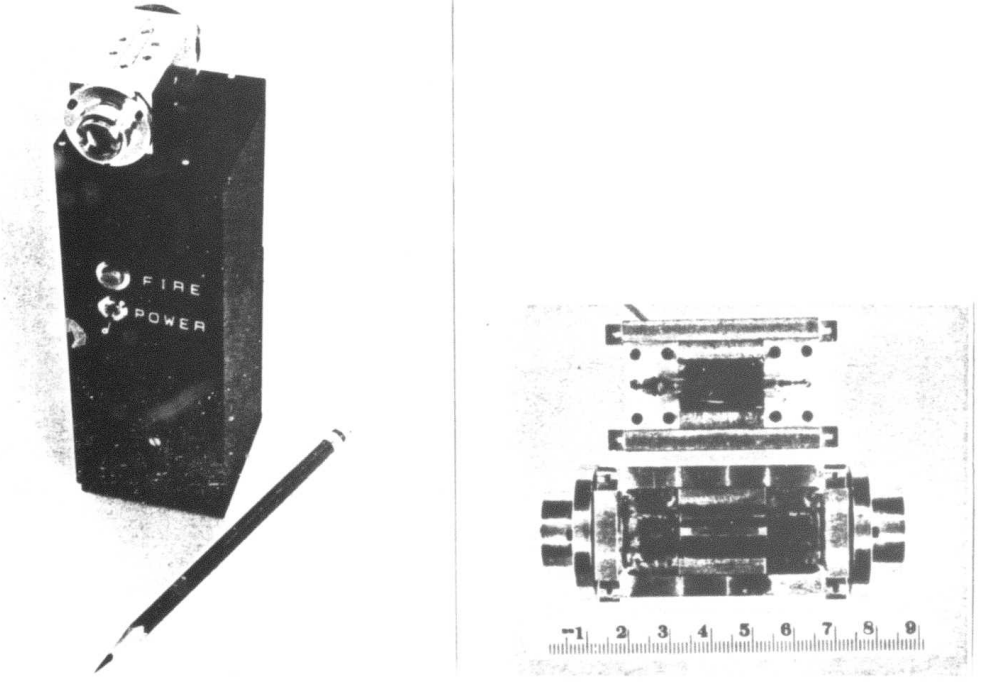


Figure 21. Hand held laser setup (SHH) and its laser head showing pump cavity (coated with Kodak white reflectance coating 6080) flashlamp, NPP rod, KSF filter, and Q-switch.

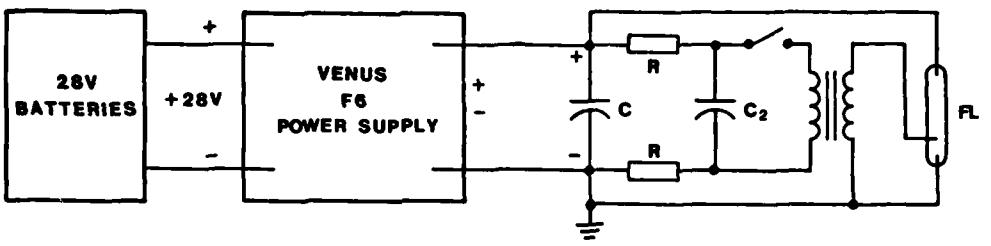


Figure 22. Flashlamp power circuitry for hand-held laser set up (SHH).

### 4.2.2 Laser Output Properties

The laser output measurements were made with an NPP laser rod, having dimensions slightly less than or about 2 x 2 x 20 mm, in the previously mentioned laser setups and cavities. The main output properties studied were laser pulse energies, pulse shapes, and beam divergences at different repetition rates with or without Q-switching. The data in this section summarizes the results and the conditions at which the results were obtained.

The highest output energies obtained with a high efficiency Type H flashlamp in the SE experimental setup was 36 mJ at 4 J of electrical input energy. This output corresponds to an overall laser efficiency of 0.9%. The parameters and other data points for this measurement are shown in Figure 23.

The highest output energies obtained with a Type L flashlamp in both the SE experimental setup and the laser head (powered by external power supply) of the SHH hand-held setup ranged between 180-190 mJ. These energies were obtained with 75-100 J of electrical input energy which corresponds to an overall laser efficency of about 0.20-0.25%. This low efficiency is most probably due to the long pump pulse duration and poor lamp performance. The parameters and other data points for these measurements in the SHH setup are shown in Figure 24. The maximum energy observed from a 2 x 2 x 20 mm NPP laser rod was 240 mJ in a special cavity containing five Type L lamps.

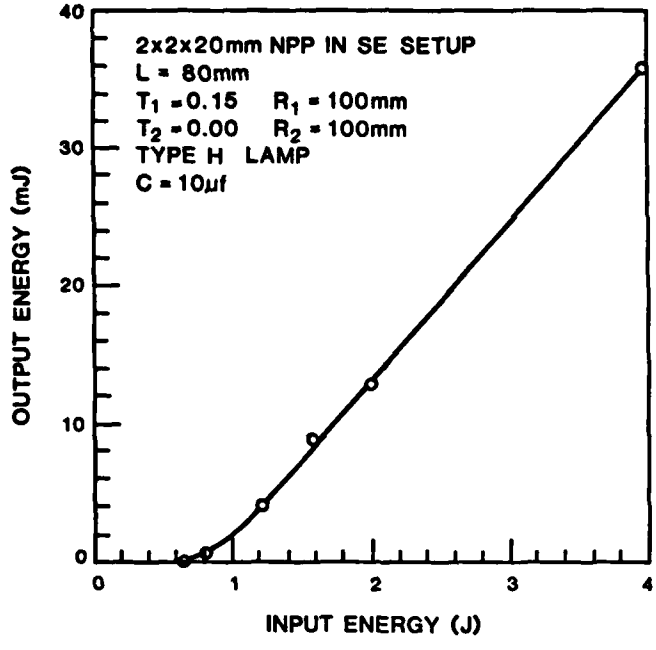


Figure 23. Output vs. input energy for NPP laser with Type H lamp in experimental setup (SE).

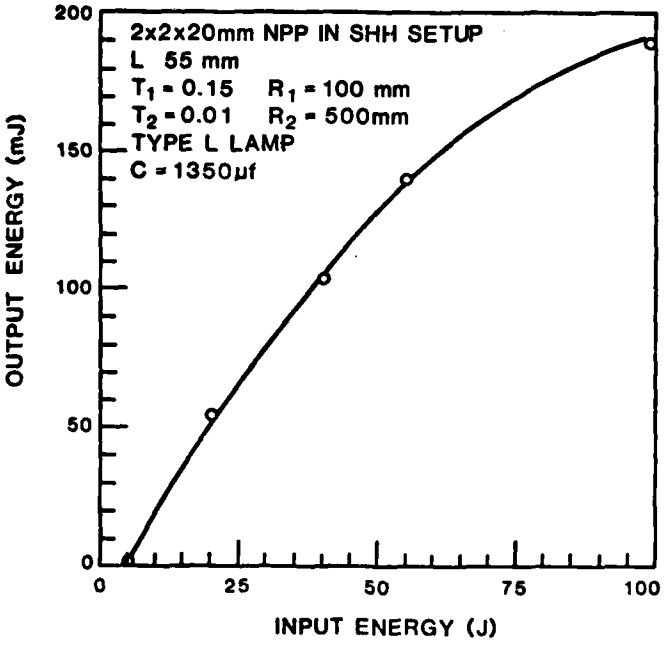


Figure 24. Output vs. input energy for NPP laser with Type L lamp in hand-held setup laser head with external power supply.

During various experiments with the Q-switched NPP lasers, it was found that with the passive Q-switch used (Eastman Kodak 15064), the efficiencies of conversion were between 10-20%; this was expected (see Ref. 18). Thus, to obtain higher-energy Q-switched output pulses, we used Type L flashlamps which can deliver high energy excitation without failure. The best results of the experiments with these flashlamps in the SE experimental setup are summarized in Table 5. Figure 25 gives typical pulse shapes for the free oscillation and the Q-switched laser output pulses obtained from these experiments.

TABLE 5. Energies of Q-switched NPP Laser Output Pulses.

| Input Energy (J) | Output Energy | |
|---|---|---|
| | Free Oscillation (mJ) | Q-Switched (mJ) |
| 59 | 110 | 17 |
| 75 | 180 | 30 |

Laser Parameters:
2x2x20 mm NPP in SE setup
L = 100 mm
$T_1$ = 0.05 $R_1$ = 100 mm
$T_2$ = 0.00 $R_2$ = 100 mm
Type L lamp, C = 1350 $\mu$F

Various experiments were conducted to operate the NPP laser at high repetition rates. The experiments were limited to the Type H flashlamps because the Type L flashlamps failed at repetition rates higher than 1 pps due to their high-energy requirements. During the experiments, it was found that without any cooling, operation of the laser in the SE setup for one minute was limited to 1 pps at free-oscillation output energies of about 10-20 mJ. When the laser was operated at 5 pps, the output energy decreased from an initial value of about 10 mJ to half of that in about 6 sec, as shown in Figure 26. The maximum number of pulses obtained from such experiments in a nearly confocal cavity was about 50. At these high repetition rates with no cooling, we observed thermal lensing in the cavity, and the output energy

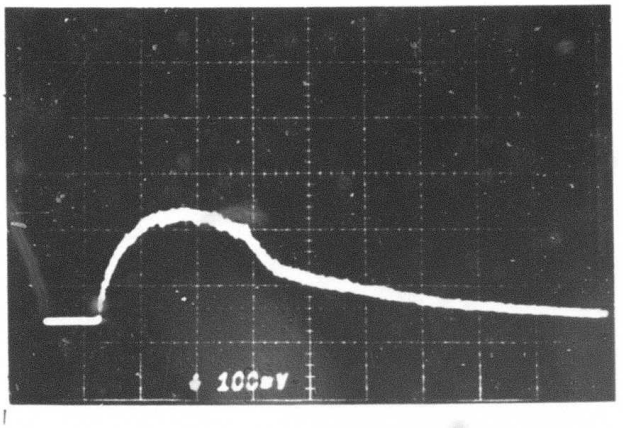

(a) Free Oscillation Mode (100 $\mu$s/div).

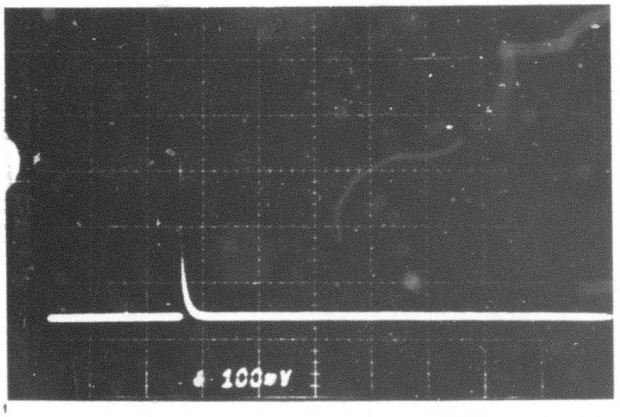

(b) Q-switched mode (100 $\mu$s/div).

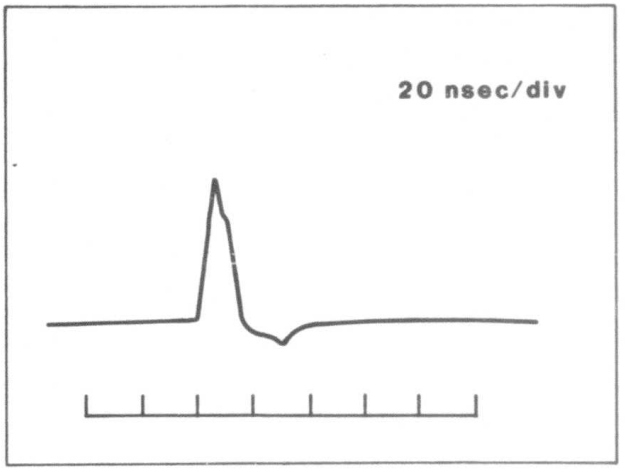


(c) Detail of Q-switched pulse.

Figure 25. Pulse shapes of laser output in Q-switched and free oscillation modes in setups described in Table 5.

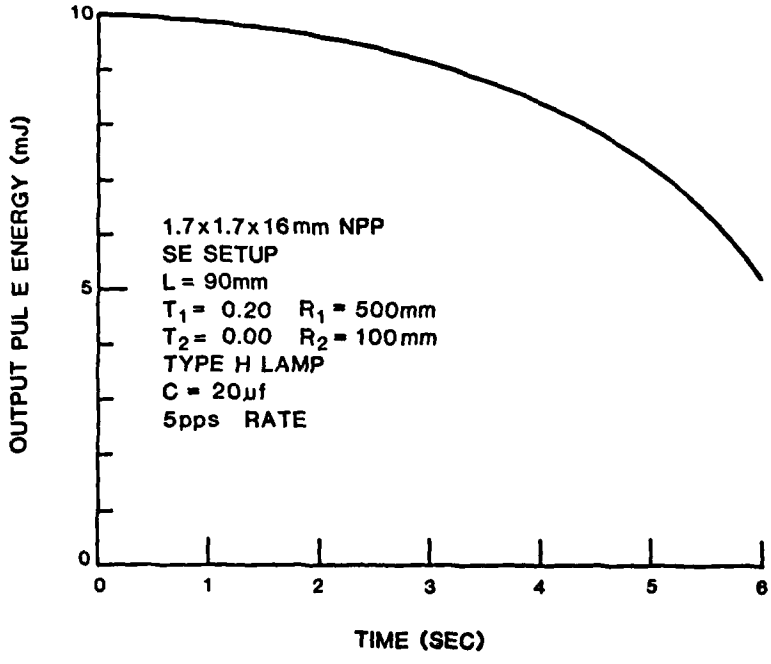


Figure 26. Typical decay of NPP laser output energy with time at a rate of 5 pps without cooling.

degraded in time (see Fig. 26) due to heating which increased the ground state absorption losses (Ref. 19). When the laser was cooled with forced argon gas, it operated at 5 pps for a few minutes with about 8 mJ average output energy. At 10 pps and with argon gas cooling, the laser still operated for a few minutes, but the average output pulse energy was much lower (less than or about 1 mJ). During these high repetition rate experiments at high input energies, no damage to the NPP laser rods due to mechanical or thermal stresses was observed. After a burst of high rate pulses, the laser recovered its properties completely following a short period of natural cooling (~1 minute).

The divergence of the output beam basically depends on the curvatures of the cavity mirror. With nearly flat cavity mirrors, it was possible to obtain a far-field beam angle of about 2 mrad (see Ref. 20). The transverse mode structure of the output for free oscillation and Q-switched operation showed a nearly fundamental Gaussian nature in most of the experiments.

## 4.3 Spectroscopic Properties of $Er_xGd_{1-x}P_5O_{14}$, $Er_xGd_{1-x}LiP_4O_{12}$, and $Er_xGd_{1-x}Al_3(BO_3)_4$

The absorption and emission properties of stoichiometric $Er^{3+}$ crystals $Er_xGd_{1-x}P_5O_{14}$, $Er_xGd_{1-x}LiP_4O_{12}$, and $Er_xGd_{1-x}Al_3(BO_3)_4$ were studied for various concentrations of $Er^{3+}$. The luminescence lifetime of the $Er^{3+}$ $^4I_{13/2}$ and $^4S_{3/2}$ levels were measured, and the decay characteristics of the $^4I_{13/2}$ --> $^4I_{15/2}$ transition were also studied at different $Er^{3+}$ concentrations. Approximate emission cross sections for both $^4S_{3/2}$ --> $^4I_{9/2}$ and $^4I_{13/2}$ --> $^4I_{15/2}$ were calculated. This section summarizes these results and evaluates these materials for lasing in the eye-safe region.

The transmission spectra of $ErP_5O_{14}$, $ErLiP_4O_{12}$, and $ErAl_3(BO_3)_4$ samples are given in Figure 27. The samples were crystalline platelets of about 0.5 mm thickness and 3 x 3 mm in area. The arbitrarily shaped background losses are probably due to the platelets being composed of smaller crystals having some inclusions. The approximate location of $Er^{3+}$ state energies in the three stoichiometric materials were obtained from the absorption spectra and are tabulated in Table 6. The energy levels in the crystals are similar to each other. Thus, Figure 28 shows an approximate level diagram for the locations of the level energies.

The previously observed laser transitions of $Er^{3+}$ in other hosts above 1.5 m are between $^4S_{3/2}$ --> $^4I_{9/2}$ ($\sim$1.7 $\mu$m), $^4I_{13/2}$ --> $^4I_{15/2}$ ($\sim$1.6 $\mu$m), and $^4I_{11/2}$ --> $^4I_{13/2}$ ($\sim$2.8 $\mu$m) (see Ref. 21). These transitions in the present materials correspond to wavelengths of about $\sim$1.7, $\sim$1.55, and $\sim$2.7 $\mu$m, respectively. Due to the limitation of our detection system, we were only able to study emissions below 1.9 $\mu$m. The spectra obtained from such emission studies did not show any fluorescence due to $^4S_{3/2}$ --> $^4I_{9/2}$ transitions near 1.7 $\mu$m in samples with full $Er^{3+}$ concentration. This indicates strong phonon-assisted cross relaxation of the $^4S_{3/2}$ --> $^4I_{9/2}$ transition to the $^4I_{15/2}$ --> $^4I_{13/2}$ transition and the $^4S_{3/2}$ --> $^4I_{13/2}$ transition to $^4I_{15/2}$ --> $^4I_{9/2}$ transition in $ErP_5O_{14}$, $ErLiP_4O_{12}$, and $ErAl_3(BO_3)_4$. This degrades the properties of four level laser action in these materials at $^4S_{3/2}$ --> $^4I_{9/2}$ transition at full $Er^{3+}$ concentrations.

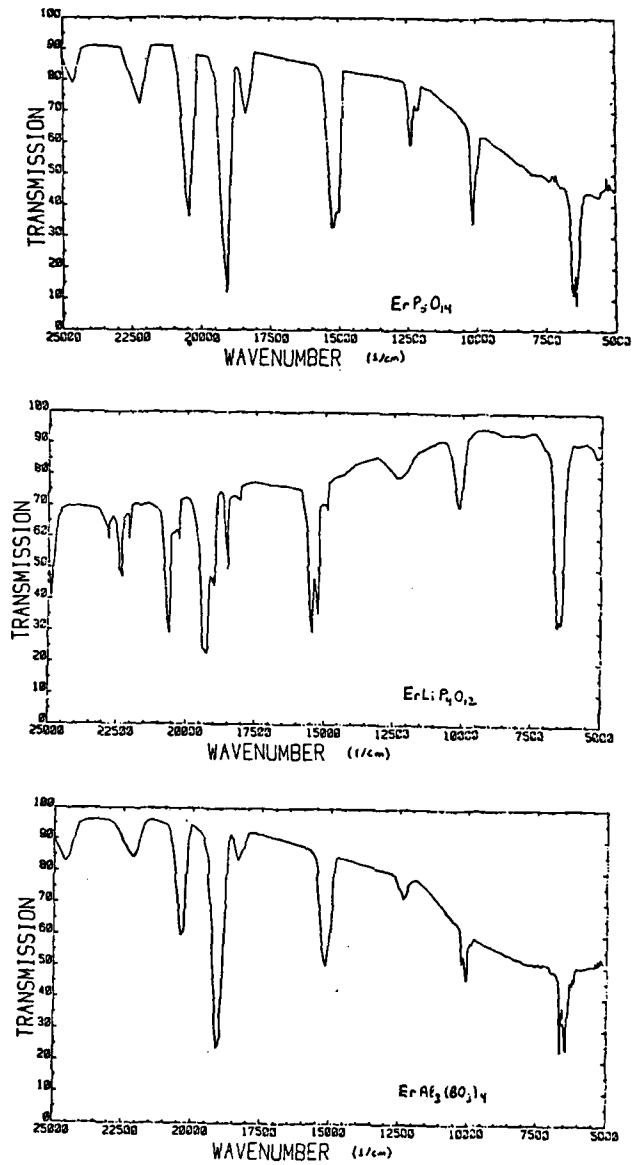


Figure 27. Transmission spectra of $ErP_5O_{14}$, $LiErP_4O_{12}$, and $ErAl_3(BO_3)_4$ in the visible and near infrared.

**TABLE 6. Level Energies of $Er^{3+}$ at 300°K.**

| Transition from $^4I_{15/2}$ to: | Energy* ($cm^{-1}$) $ErP_5O_{14}$ | $ErLiP_4O_{12}$ | $ErAl_3(BO_3)_4$ |
|---|---|---|---|
| $^4I_{13/2}$ | 6450 | 6500 | 6550 |
| $^4I_{11/2}$ | 10200 | 10100 | 10200 |
| $^4I_{9/2}$ | 12400 | 12300 | 12400 |
| $^4F_{9/2}$ | 15200 | 15300 | 15300 |
| $^4S_{3/2}$ | 18300 | 18400 | 18400 |
| $^2H_{11/2}$ | 19100 | 19200 | 19200 |
| $^4F_{7/2}$ | 20500 | 20600 | 20400 |
| $^4F_{5/2}$, $^4F_{3/2}$ | 22200 | 22300 | 22100 |
| $^2H_{9/2}$ | 24700 | 24900 | 24600 |

(*) Effective linewidths at 300°K are between 200-500 $cm^{-1}$.

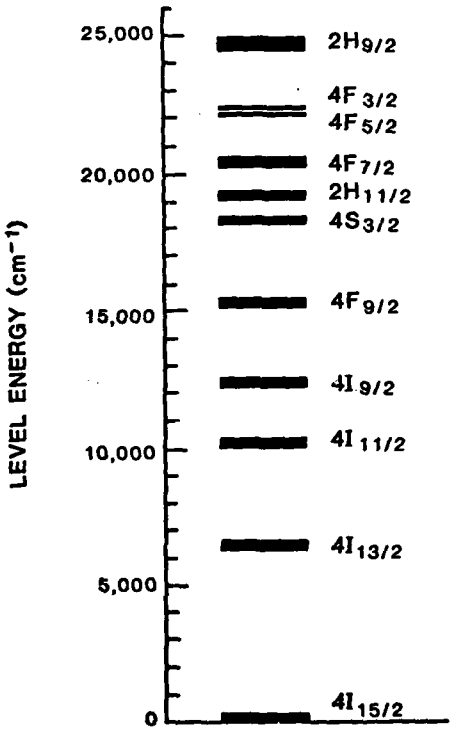


Figure 28. Approximate level diagram of $Er^{3+}$ in $ErP_5O_{14}$, $ErLiP_4O_{12}$, and $ErAl_3(BO_3)_4$.

We tried to observe $4S_{3/2}$ --> $4I_{9/2}$ emission at very low $Er^{3+}$ concentrations in materials diluted by Gd [in $Er_{0.004}Gd_{0.996}P_5O_{14}$, and $Er_{0.04}Gd_{0.96}Al_3(BO_3)_4$], but due to the low levels of $Er^{3+}$ no emission was detected. The emission spectra due to $4I_{13/2}$ --> $4I_{15/2}$ transition in fully $Er^{3+}$ concentrated materials are shown in Figure 29. All of these spectra are similar at room temperature and do not change considerably for low $Er^{3+}$ concentrations.

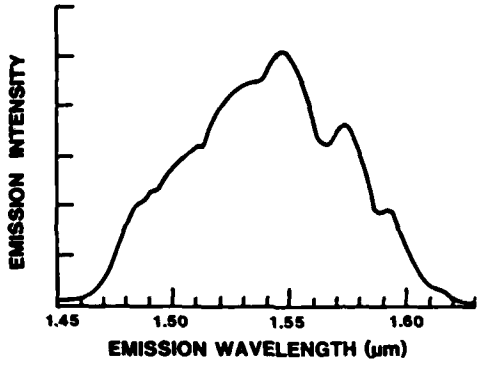


(a) $ErP_5O_{14}$.

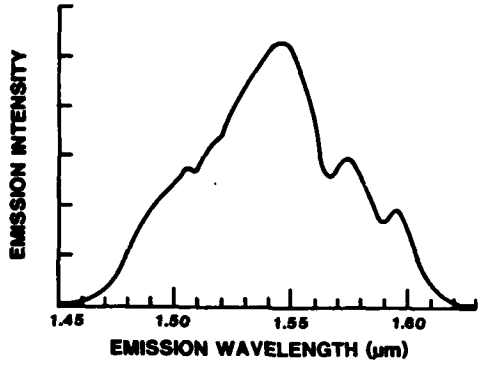


(b) $LiErP_4O_{12}$.

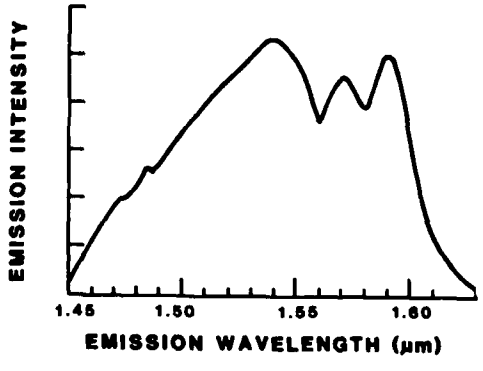


(c) $ErAl_3(BO_3)_4$.

Figure 29. Emission spectra of $ErP_5O_{14}$, $LiErP_4O_{14}$, and $ErAl_3(BO_3)_4$ in eye-safe region.

The fluorescence lifetimes of $Er^{3+}$ $4I_{13/2}$ state in all three materials diluted with different concentrations of $Gd^{3+}$ were measured. The data is given in Table 7. The concentration of $Er^{3+}$ and $Gd^{3+}$ in these materials were assumed to be the same as the compositional ratio of the starting flux for crystal growth. This was checked in the case of $Er_xGd_{1-x}P_5O_{14}$ with x-ray fluorescence, and the agreement was very good. The lifetime data shows that there is only a small amount of concentration quenching in all three materials, indicating that these crystals are good hosts for $Er^{3+}$. The fluorescence lifetimes measured for $4I_{13/2}$ state in $Er_{0.004}Gd_{0.996}P_5O_{12}$

TABLE 7. $4I_{13/2}$ --> $4I_{15/2}$ Fluorescence Lifetimes of $Er^{3+}$.

| $Er_xGd_{1-x}P_5O_{14}$ | | $Er_xGd_{1-x}LiP_4O_{12}$ | | $Er_xGd_{1-x}Al_3(BO_3)_4$ | |
|---|---|---|---|---|---|
| x | τ (ms) | x | τ (ms) | x | τ (ms) |
| 1.000 | 3.3 | 1.000 | 4.3 | 1.000 | 0.23 |
| 0.667 | 3.0 | 0.667 | 4.5 | 0.750 | 0.25 |
| 0.500 | 3.3 | 0.500 | 5.4 | 0.500 | 0.27 |
| 0.333 | 3.5 | 0.330 | 5.8 | 0.250 | 0.27 |
| 0.150 | 4.8 | 0.100 | 6.4 | 0.040 | 0.29 |
| 0.004 | 5.0 | | | | |

and $Er_{0.1}Gd_{0.9}LiP_4O_{12}$ are very close to their calculated radiative lifetimes (Refs. 22,23). We measured the lifetime of the $4S_{3/2}$ state in $ErP_5O_{14}$, and the result was much shorter than its radiative value, indicating the heavy cross-relaxation previously mentioned.

It is seen from the data given in this section that the eye-safe emission from $Er^{3+}$ in the three materials studied is observed from the $4I_{13/2}$ --> $4I_{15/2}$ transition. In other hosts this transition has shown lasing at both 300°K and 77°K, with typical thresholds less than 50 J/cm (Ref. 24). $4I_{13/2}$ --> $4I_{15/2}$ is a transition for a three-level laser scheme, and normally requires either cooling or higher thresholds. The approximate emission cross sections of these transitions together with the fluorescence lifetimes in fully $Er^{3+}$ concentrated samples are given in Table 8. High

$Er^{3+}$ concentration helps to populate $4I_{13/2}$ states due to cross relaxation from $4S_{3/2}$ states. Otherwise the pumping of $4I_{13/2}$ is very slow due to the slow relaxation of upper levels (Ref. 26). Although no emission could be detected from the $4S_{3/2}$ --> $4I_{9/2}$ transition in the three stoichiometric crystals, a similar situation was the case in 0.5% Er:$YAlO_3$ where $4S_{3/2}$ --> $4I_{9/2}$ was lased (Ref. 25). This $4S_{3/2}$ --> $4I_{9/2}$ transition has also shown lasing in many other hosts both at room temperature and at liquid nitrogen temperatures with relatively low thresholds. Typical thresholds in other hosts are less than 10 J/cm at 300°K with low $Er^{3+}$ concentration (Ref. 24) to avoid cross relaxation. The cross section and lifetime data for the $4S_{3/2}$ --> $4I_{9/2}$ transition are also given in Table 8.

TABLE 8. Emission Cross Sections and Lifetimes of $Er^{3+}$ Eye-safe Transitions.

| Transition | Approximate Wavelength (μm) | $ErP_5O_{14}$ τ(ms) | $ErP_5O_{14}$ $\sigma_e(cm^2)$ | $ErLiP_4O_{12}$ τ(ms) | $ErLiP_4O_{12}$ $\sigma_e(cm^2)$ | $ErAl_3(BO_3)_4$ τ(ms) | $ErAl_3(BO_3)_4$ $\sigma_e(cm^2)$ |
|---|---|---|---|---|---|---|---|
| $4I_{13/2}$ --> $4I_{15/2}$ | 1.55 | 3.3 | $5 \times 10^{-21}$ | 4.3 | $4 \times 10^{-21}$ | 0.23 | $4 \times 10^{-21}$ |
| $4S_{3/2}$ --> $4I_{9/2}$ | 1.7 | 0.0007(1) | $5 \times 10^{-21}$ | 0.001(2) | $5 \times 10^{-21}$ | - | - |

(1) From our measurements. Corresponding measurements in literature are 490 ns (Ref. 26) and 1200 ns (Ref. 23).

(2) Ref. 22.

From the data given in this section, it is seen that the $Er^{3+}$ ion in all three stoichiometric crystals has a good possibility of lasing at both the four-level $4S_{3/2}$ --> $4I_{9/2}$ and the three-level $4I_{13/2}$ --> $4I_{15/2}$ eye-safe transitions. To make use of the $4S_{3/2}$ --> $4I_{9/2}$ transition, low concentrations of $Er^{3+}$ should be used to decrease the effects of cross relaxation. For the $4I_{13/2}$ --> $4I_{15/2}$ transition, however, higher $Er^{3+}$ concentrations may be desirable because cross relaxation helps to populate the $4I_{13/2}$ states. Additional studies should be conducted to understand these materials further and to achieve lasing.

## 5. CONCLUSIONS

After surveying all better known stoichiometric Nd-laser materials, we have grown crystals of the most promising candidates for a 1.06 $\mu$m miniature laser system, namely of $NdP_5O_{14}$ (NPP), $NdLiP_4O_{12}$ (LNP), and $NdAl_3(BO_3)_4$ (NAB). Subsequently, these crystals were optically evaluated.

The crystal growth experiments have shown that laser-quality $NdP_5O_{14}$ crystals up to 35 mm in cross section can be grown on a routine basis from hot phosphoric acids, and that laser rods 2 x 2 x 20 mm in size can be fabricated from such crystals, although sometimes with difficulties. The experiments have also shown that $NdLiP_4O_{12}$ crystals can be grown from fluxed melts by top or bottom seeding techniques, but with greater difficulty than the $NdP_5O_{14}$ crystals. Although crystal growth of $NdLiP_4O_{12}$ was discontinued during the middle of this program, it is felt that with an increased effort laser-quality crystals of this material, or of $NdKP_4O_{12}$, large enough for fabricating laser rods could be grown. It was shown, also, that crystals of $NdAl_3(BO_3)_4$, nearly large enough in size for fabrication of miniature laser rods, can be grown from fluxed melts. Top and bottom seeding techniques were used again; the crystals, however, were generally not free of inclusions. Because of the presently debated, possible dual-phase nature of this compound, our work on this material was discontinued in the early stages of the program.

The data presented in Section 4 of this report clearly show that NPP miniature lasers with 2 x 2 x 20 mm crystals can easily deliver 30 mJ Q-switched output pulses. The durations of similar pulses with lower energies were measured to be around 15 nsec. If no cooling is used, the repetition rates of such pulses are limited to 1 pps or less. If, however, adequate cooling is provided, our studies show that a pulse rate in the order of 5 pps is possible, and that a rate of 10 pps is possible with slightly lower output energies. The divergence of the beam does not pose a problem, since it can be adjusted easily by proper design of the laser cavity. A far-field beam angle of about 2 mrad was easily achieved by selecting a cavity design with nearly flat mirrors.

During the latter part of the contract, the Er counterparts of the above Nd compounds, diluted with various amounts of Gd or Yb were investigated as

possible candidates for a miniature laser system emitting in the eye-safe region of the spectrum.

Crystal growth experiments on $Er_x(Gd,Yb)_{1-x}P_5O_{14}$, $Er_x(Gd,Yb)_{1-x}LiP_4O_{12}$, and $Er_x(Gd,Yb)_{1-x}Al_3(BO_3)_4$ have shown that single crystals can be produced by techniques similar to those used for their Nd-counterparts. Changes in the growth procedures, however, were required. Crystals of $ErP_4O_{14}$ up to 1 cm in size were grown by our technique; this work was performed during the last four months of the contract.

The optical experiments on Er-containing stoichiometric crystals show that the properties of Er in these materials are similar to those of Er in other hosts which have shown lasing at various eye-safe transitions. In addition, the concentration quenching of luminescence from $4I_{13/2}$ levels of $Er^{3+}$ in the present materials is very small. From these similarities and properties, it is concluded that the present stoichiometric $Er^{3+}$ crystals can be used as good hosts for $Er^{3+}$ eye-safe lasers at 1.55 $\mu$m and 1.7 $\mu$m.

## 6. REFERENCES


1. R.B. Chesler and D.A. Praegent, Appl. Phys. Lett. 23, 235 (1973).

2. J.P. Budin, M. Neubauer, and M. Rondot, IEEE J. Quantum Electr., QE-14, 831 (1978).

3. R.D. Plättner, W.W. Krühler, W.K. Zwicker, T. Kovats and S.R. Chinn, J. Cryst. Growth 49, 274 (1980).

4. G. Huber and H.G. Danielmeyer, Proc. International Conf. Lasers '79, p. 619.

5. O. Jarchow, F. Lutz and K.H. Klaska, Zeit. Fur. Krist. 149, 162 (1979).

6. D. Yu. Pushcharovskii, O.G. Karpov, N.I. Leonyuk and N.V. Belov, Sov. Phys. Dokl. 23, 450 (1978).

7. G. Huber, Current Topics in Materials Science, Vol. 4, Ed. E. Kaldis, North Holland, p. 23, (1980).

8. F. Kellendonk, M.A. van Os and S. Blasse, Chemical Physics Letts. 61, 239 (1979).

9. L.I. Al'shinskaya, N.I. Leonyuk and T.I. Timchenko, Krist und Tech. 14, 897 (1979).

10. L.I. Al'shinskaya, T.I. Timchenko and A.A. Lipatova, Vert. Moskov, Univ. Geol. 32, 120 (1977).

11. L.I. Mallseva, N.I. Leonyuk and T.I. Timchenko, Krist und Tech. 15, 35 (1980).

12. N.I. Leonyuk, A.V. Pashkova and N.V. Belov, Krist und Tech. 14, 47 (1979).

13. V.I. Bilak, I.I. Kurater, N.I. Leonyuk, V.A. Pachkor, A.V. Pashkova, T.I. Timchenko and A.V. Shestokov, Sov. Phys. Dokl. 23, 299 (1978).

14. T.I. Timchenko, N.I. Leonyuk, A.V. Pashkova and O.L. Zhurovleva, Sov. Phys. Dokl. 24, 336 (1979).

15. Philips Laboratories, Development of a Novel Laser Material for Miniaturized Laser Systems, W.K. Zwicker et al., Qtly. Tech. Report, Jan-Mar 1981, DARPA Contract No. MDA903-81-C-0034.

16. Philips Laboratories, Development of a Novel Laser Material for Miniaturized Laser Systems, W.K. Zwicker et al., Qtly. Tech. Report, Nov-Dec 1980, DARPA Contract No. MDA903-81-C-0034.

17. Philips Laboratories, Development of a Novel Laser Material for Miniaturized Laser Systems, W.K. Zwicker et al., Qtly. Tech. Report, Apr-Jun 1981, DARPA Contract No. MDA903-81-C-0034.

18. S.R. Chinn, Research Studies on NPP Miniature Lasers, MIT Lincoln Lab, Final Report (1978).

19. S.R. Chinn, W.K. Zwicker, and S. Colak, "Thermal Behavior of $NdP_5O_{14}$ Lasers", to be published in J. Appl. Phys.

20. Philips Laboratories, Development of a Novel Laser Material for Miniaturized Laser Systems, W.K. Zwicker et al., Qtly. Tech. Report, Jul-Sep 1981, DARPA Contract No. MDA903-81-C-0034.

21. M.J. Weber, "Rare Earth Lasers", in Handbook on the Physics and Chemistry of Rare Earths, Ed. K.A. Gschneidner, North Holland, 1979.

22. W. Ryba-Romanowski, Z. Marzuak, B. Jezowska-Trzebiatowska, D. Schutze, and Ch. Waligara, "Growth and Spectroscopic Properties of $LiErP_4O_{12}$ Single Crystals", Phys. Stat. Sol. (a), 62, 75 (1980).

23. Z. Mazurak, W. Ryba-Romanowski, B. Jezowska-Trzebiatowska, "Radiative and Nonradiative Transitions in $ErP_5O_{14}$ Single Crystals", J. Luminescence, 17, 401 (1978).

24. A.A. Kaminskii, Laser Crystals, Springer-Verlag, 1981.

25. W.J. Weber, M. Bass, and G.A. DeMars, "Laser Action and Spectroscopic Properties of $Er^{3+}$ in $YALO_3$", J. Appl. Phys., 42, 301 (1971).

26. H. Pruss, Thesis, University of Hamburg, (1980).

## DISTRIBUTION LIST

| | Copies |
|---|---|
| Director<br>Defense Advanced Research Projects Agency<br>Attention: TIO/Admin.<br>1400 Wilson Blvd.<br>Arlington, Virginia 22314 | (3) |
| Dr. James Gibson<br>DELNV-L<br>Night Vision & Electro-Optics Laboratories<br>Fort Belvoir, Virginia 22060 | (1) |
| Defense Documentation Center<br>Cameron Station<br>Alexandria, Virginia 22314 | (12) |
| TACTEC<br>Battelle Memorial Institute<br>505 King Avenue<br>Columbus, Ohio 43201 | (1) |